2005

Evolution of the magmatic-hydrothermal acid-sulfate system at Summitville, Colorado: integration of geological, stable-isotope, and fluid-inclusion evidence

Philip M. Bethke
U.S. Geological Survey, Reston, Virginia

Robert O. Rye
U.S. Geological Survey, Denver, Colorado, rrye@usgs.gov

Roger E. Stoffregen
305 Swissvale Avenue, Pittsburgh, Pennsylvania

Peter G. Vikre
U.S. Geological Survey, Reno, Nevada

ELSEVIER

Chemical Geology 215 (2005) 281–315

CHEMICAL GEOLOGY
INCLUDING
ISOTOPE GEOSCIENCE

www.elsevier.com/locate/chemgeo

Evolution of the magmatic-hydrothermal acid-sulfate system at Summitville, Colorado: integration of geological, stable-isotope, and fluid-inclusion evidence

Philip M. Bethke[a,*], Robert O. Rye[b], Roger E. Stoffregen[c], Peter G. Vikre[d]

[a]*U.S. Geological Survey, Reston, Virginia 20192, U.S.A.*
[b]*U.S. Geological Survey, Denver, Colorado 80225, U.S.A.*
[c]*305 Swissvale Avenue, Pittsburgh, Pennsylvania 15218, U.S.A.*
[d]*U.S. Geological Survey, Reno, Nevada 89557, U.S.A.*

Accepted 1 June 2004

Abstract

The Summitville Au–Ag–Cu deposit is a classic volcanic dome-hosted high-sulfidation deposit. It occurs in the Quartz Latite of South Mountain, a composite volcanic dome that was emplaced along the coincident margins of the Platoro and Summitville calderas at 22.5±0.5 Ma, penecontemporaneous with alteration and mineralization. A penecontemporaneous quartz monzonite porphyry intrusion underlies the district and is cut and overlain by pyrite–quartz stockwork veins with traces of chalcopyrite and molybdenite.

Alteration and mineralization proceeded through three hypogene stages and a supergene stage, punctuated by at least three periods of hydrothermal brecciation. Intense acid leaching along fractures in the quartz latite produced irregular pipes and lenticular pods of vuggy silica enclosed sequentially by alteration zones of quartz–alunite, quartz–kaolinite, and clay. The acid-sulfate-altered rocks host subsequent covellite + enargite/luzonite + chalcopyrite mineralization accompanied by kaolinite, and later barite–base-metal veins, some containing high Au values and kaolinite.

The presence of both liquid- and vapor-rich fluid inclusions indicates the episodic presence of a low-density fluid at all levels of the system. In the mineralized zone, liquid-rich fluid inclusions in healed fractures in quartz phenocrysts and in quartz associated with mineralization homogenize to temperatures between 160 and 390 °C (90% between 190 and 310 °C), consistent with the range (200–250 °C) estimated from the fractionation of sulfur isotopes between coexisting alunite and pyrite. A deep alunite–pyrite pair yielded a sulfur-isotope temperature of 390 °C, marking a transition from hydrostatic to lithostatic pressure at a depth of about 1.5 km.

Two salinity populations dominate the liquid-rich fluid inclusions. One has salinities between 0 and 5 wt.% NaCl equivalent; the other has salinities of up to 43 wt.% NaCl equivalent. The occurrence of high-salinity fluid inclusions in vein quartz associated with mineralization, as well as in the deep stockwork veins, suggests that brines originating deep in the system transported the metals.

* Corresponding author: Tel.: +1 703 648 6181; fax: +1 703 648 6783.
E-mail address: pbethke@usgs.gov (P.M. Bethke).

0009-2541/$ - see front matter
doi:10.1016/j.chemgeo.2004.06.041

The $\delta^{34}S$ values of sulfides in magnetite (−2.3‰) and of sulfate in apatite (5.4‰) in unaltered quartz latite indicate that $\delta^{34}S_{\Sigma S}$ was near 0‰. The $\delta^{34}S$ values of coexisting alteration alunite and pyrite are 18.2‰ to 24.5‰ and −8.1‰ to −2.2‰, respectively. Deep in the system, most of the change in $\delta^{34}S$ values occurs in the sulfates, indicating that the fluids were initially H_2S-dominant, their redox state buffered at depth by equilibration with igneous rocks. However, in the main alteration zone, most of the change in $\delta^{34}S$ values occurs in pyrite, indicating that the fluids moved off the rock buffer and became SO_4^{2-}-dominant as pyrite precipitated and SO_2 disproportionation produced the sulfuric acid requisite for acid leaching. The $\delta^{34}S$ values of the late-stage barite and sulfides indicate that the system returned to high H_2S/SO_4^{2-} ratios typical of the original rock-buffered fluid.

The δD_{H2O} of alunite parent fluids was near −45‰ and their $\delta^{18}O$ ranged from 7‰ to −1‰, depending on the degree of exchange in the alteration zone at low water–rock ratio, or mixing with unexchanged meteoric water. The low δD values of some alunite samples are interpreted to result from postdepositional exchange with later ore fluids.

Fluid exsolved from the magma at depth had δD_{H2O} and $\delta^{18}O_{H2O}$ values near −70‰ and 10‰, respectively. During and following migration to the top of the magma chamber, the fluid underwent isotopic exchange with the partially crystallized magma and its solid and cooler, but still plastic, carapace just below the transition from a lithostatic to hydrostatic pressure regime. These *evolved magmatic* fluids had δD_{H2O} and $\delta^{18}O_{H2O}$ values close to −40‰ and 5‰, respectively, prior to release into the superjacent hydrostatically pressured fracture zone, wherein the fluids separated into a low-density phase and hypersaline brine. The low-density phase rose to the level of acid-sulfate alteration, where disproportionation of SO_2 commenced upon condensation of the vapor plume causing the acid-sulfate alteration. Hydrogen and oxygen isotopic compositions estimated from deep kaolinitic wallrock alteration and fluid inclusions in quartz stockwork veins indicate the brine mixed with highly exchanged meteoric water at depth and rose to the ore zone, producing the Cu–Au–Ag mineralization. The composition of inclusion fluids in a single sample of enargite also indicates mixing between ore fluids and unexchanged meteoric water at shallow depths. The sulfate in fluids responsible for precipitation of most barite samples was of magmatic origin, but the $\delta^{34}S$ of a single sample suggests mixing with sulfate derived from the atmospheric oxidation of H_2S in an overlying steam-heated zone.

Keywords: Alunite; Stable isotopes; Fluid inclusions; High-sulfidation; Epithermal; Summitville, Colorado

1. Introduction

The Au–Ag–Cu deposit at Summitville in southwestern Colorado is an archetypal example of a volcanic dome-hosted magmatic-hydrothermal epithermal deposit characterized by intense acid-sulfate alteration and a high-sulfidation assemblage of sulfide minerals (Bethke, 1984; Hayba et al., 1985). Among the attributes that make Summitville a classic example of such deposits are its relatively small size (17.4 tonnes or ~560,000 oz Au), simple geometry and volcanic history, spectacular alteration zoning, and the preservation of a full vertical range of features that encompass weak porphyry-style mineralization, encountered in deep exploration drilling, to surficial sinter deposits.

Interpretation of the alteration and ore-forming processes at Summitville is further facilitated by the large base of knowledge of the geology, mineralogy, and geochemistry of the district (Steven and Ratté, 1960; Stoffregen, 1985, 1987; Gray and Coolbaugh, 1994). In addition, extensive environmental studies at Summitville have made it a type example of the environmental impact of the weathering of such deposits in both natural and mine-related exposure (Gray et al., 1994).

Deposits having similar volcanic association and alteration and ore mineral assemblages have been variously referred to in the literature as *Goldfield-type* (Steven and Ratté, 1960; Bethke, 1984), *enargite–gold* (Ashley, 1982), *quartz–alunite gold* (Berger, 1986), *acid-sulfate* (Heald-Wetlaufer et al., 1987), *high-sulfidation* (Hedenquist, 1987), and *kaolinite–alunite* (Berger and Henley, 1989). The designation "*high-sulfidation*", used in reference to the sulfidation state of the ore-mineral assemblage (Barton and Skinner, 1979), has been generally accepted. Such designation is not without ambiguity, however, because not all deposits that contain "high-sulfidation" minerals (enargite–luzonite–covellite–pyrite) are of the Summitville

type, and perhaps the modifier "epithermal" should be included for clarity.

The association of Au mineralization with advanced argillic alteration in or adjacent to volcanic domes has been reported from many areas of Cenozoic volcanism, such as Chinkuashi, Taiwan (Huang, 1955), Goldfield, Nevada (Ashley, 1974; Vikre, 1990), Julcani, Peru (Deen, 1990), and Pierina, Peru (Fifarek and Rye, this issue); other examples are given by White and Hedenquist (1995), Sillitoe (1989), and in the comprehensive review by Arribas (1995). Less commonly, this association is preserved in older rocks, as at the 1.8 Ga Tapajós deposit in Brazil (Juliani et al., this issue), the mid-Paleozoic Mt. Leyshon deposit in Australia (Scott, 1990) and the Hope Brook deposit in Newfoundland, Canada (Dubé et al., 1998).

Isotopic studies of the Summitville district, begun in early 1984, were seminal in the development of the stable-isotope systematics of acid-sulfate alteration that accompanies precious-metal mineralization in high-sulfidation deposits and the acid-sulfate alteration in various other geological environments (Rye et al., 1990, 1992; Rye, 1993). Among the important advances by these studies were: (1) development of techniques for total stable-isotope analyses of alunite (Wasserman et al., 1992); (2) determination of experimental alunite–water isotope fractionation factors (Stoffregen et al., 1994); and (3) isotopic investigation of similar high-sulfidation deposits, thus leading to the development of conceptual genetic models and to the understanding of the principles of stable-isotope geochemistry of such deposits (e.g., Rye et al., 1989, 1992; Bove et al., 1990; Deen et al., 1994; Hedenquist et al., 1994: Arribas et al., 1995).

Since completion of the initial isotopic study of Summitville (Rye et al., 1990), much has been learned about the evolution of magmatic fluids and the processes that occur at high levels in the magmatic-hydrothermal acid-sulfate environment leading to formation of deposits like Summitville. It is now generally accepted that such deposits form in the magmatic-hydrothermal environment as defined by Rye et al. (1992). The application of detailed fluid-inclusion studies and stable-isotope techniques, together with careful field and petrographic studies, has added considerable depth to our understanding of these processes. Here, we integrate stable-isotope and fluid-inclusion studies with the geological and geochemical documentation of the Summitville district, and discuss new insights regarding the evolution of magmatic fluids and their interaction with meteoric water during alteration and mineralization.

The conclusion of mining at Summitville in 1991 was followed by serious downstream environmental damage due to acid mine drainage (Gray et al., 1994). This problem resulted primarily because pervasive alteration of the host rocks had formed highly siliceous and argillized assemblages with little capacity to neutralize acidic waters generated during weathering of the relatively small amount (<5%) of sulfide in the rocks. In hindsight, had the presently available geological and geochemical information on the Summitville deposit been integrated with environmental characterization studies, more effective efforts could have been taken to mitigate the environmental impact of mining. Geological and geochemical studies such as this one are thus an essential initial process in an environmental characterization of a mineral deposit, and are critical to understanding the effect of mining on the environment.

2. Geological and mineralogical framework of the Summitville deposit

Exploration drilling and open-pit mining subsequent to the work of Steven and Ratté (1960) exposed the Summitville deposit over a vertical range of more than a kilometer and allowed drillhole logging and high-wall mapping and sampling on which the detailed studies by Stoffregen (1985, 1987), Gray and Coolbaugh (1994), and Getahun (1994) were based. These studies, along with the classic study by Steven and Ratté (1960) and the earlier studies of Hills (1885) and Patton (1917), should be consulted for a complete description of the geological framework, mineral paragenesis, and history of development of the deposit; only a brief summary is given here.

Summitville is at an elevation of about 3750 m in the Summitville–Platoro caldera complex in the mid-Tertiary San Juan volcanic field in southwestern Colorado (Fig. 1). Ore is hosted almost entirely by the coarsely porphyritic core phase of the composite South Mountain volcanic dome (formally the Quartz Latite of South Mountain, but more conveniently

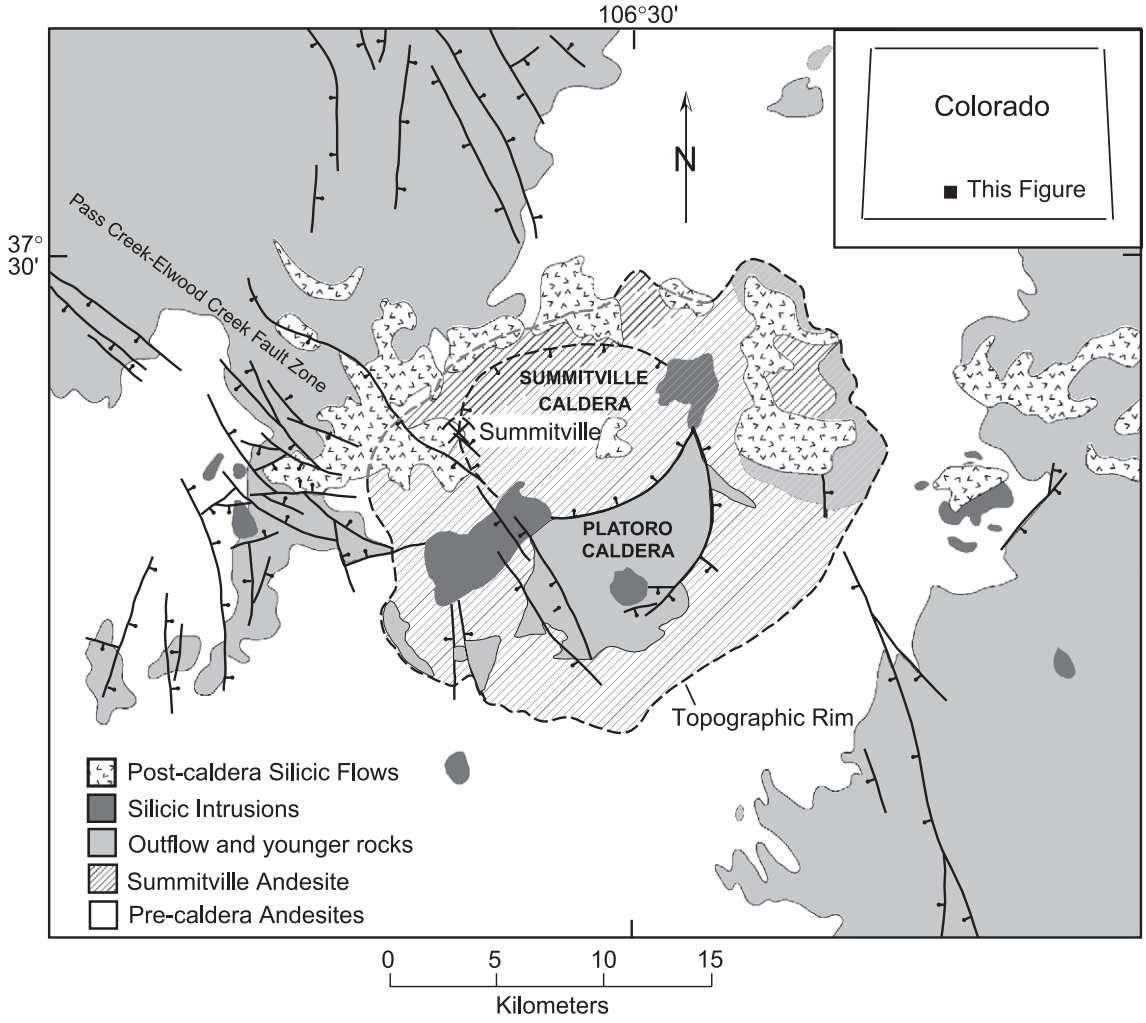

Fig. 1. Generalized geology of the area of the Platoro–Summitville calderas, showing the location of Summitville with respect to the Platoro and Summitville calderas and the Pass Creek–Elwood Creek fault zone. Topographic wall of the Platoro caldera and structural wall of the Summitville caldera are shown. Hachures are on the downthrown side of faults. Modified from Steven and Lipman (1976).

referred to as the South Mountain quartz latite). The dome was emplaced along the coincident margins of the Platoro caldera and the younger, nested Summitville caldera at their intersection with the NW-trending Pass Creek–Elwood Creek fault zone. The South Mountain dome is cut by two major faults; on the south by the unmineralized South Mountain Fault, which is a component of the Pass Creek–Elwood Creek fault zone, and on the north by the mineralized Missionary Fault, which forms the contact of the dome with the surrounding caldera-filling Summitville andesite.

Alteration and mineralization at Summitville formed fault-controlled, subvertical tabular zones and pods within the South Mountain quartz latite (Figs. 2 and 3). Economic gold mineralization occurs between 3566 and 3720 m elevation, but drilling showed that the hydrothermal system extended over a vertical range of more than 1800 m. Deep core drilling by ASARCO in the mid-1970s intercepted an equigranular quartz monzonite intrusion beneath the district at an elevation of approximately 3250 m, nearly 400 m below the lowest level of the open pit. The quartz monzonite is altered to a quartz+'sericite'+pyrite±kaolinite assem-

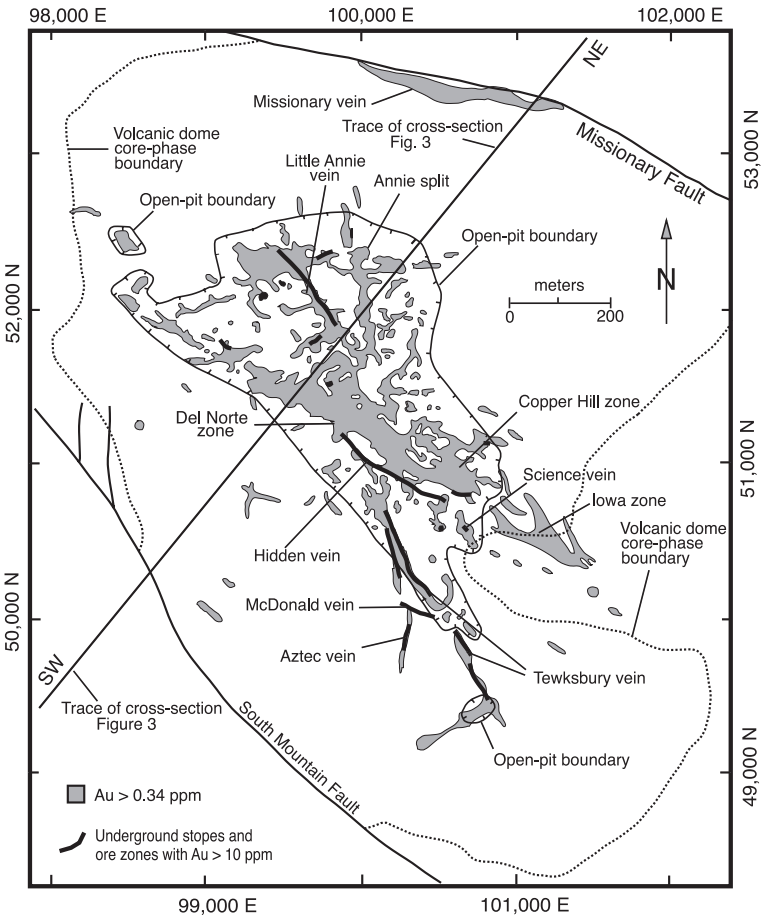

Fig. 2. Plan view of Summitville mine area, showing the location of mine areas and veins referred to in the text, the outer boundary of the core phase of the South Mountain volcanic dome, the South Mountain and Missionary fault zones, the distribution of mineable Au values (>0.34 g t^{-1}), and the areas of high Au values (>10 g t^{-1}). The linearity of patterns for Au values reflects the subvertical tabular nature of intersecting fault-controlled vuggy-silica and surrounding quartz–alunite and quartz–kaolinite alteration zones. After Gray et al. (1994).

blage and contains stockwork pyrite–quartz veins with trace amounts of chalcopyrite and molybdenite. According to Enders and Coolbaugh, (1987), the quartz monzonite intrudes the South Mountain quartz latite.

The upper limits of alteration and (or) mineralization can be reasonably constrained geologically. Steven and Ratté (1960) placed the present elevation of the paleosurface above the ore zone between ~3900 m (the projected surface of the 20 Ma Cropsy Rhyolite) and 4145 m (the restored top of the South Mountain dome in their cross section). Enders and Coolbaugh (1987) cited the occurrence of cristobalite–opal replacements and associated silica sinter containing plant fragments on the downthrown block of the South Mountain Fault southwest of the deposit as evidence of a regional paleosurface. Adjusting for ~100 m of displacement on the South Mountain Fault (Steven and Ratté, 1960), the sinter was deposited on the flank of the dome at an approximate present elevation of 3900 m. Considered together with the close temporal relationship between the emplacement of the dome and alteration–mineralization, these observations suggest that the paleosurface above the ore zone was close to 4145 m present elevation (the restored top of the dome). The highest mine workings are the Aztec glory hole at 3749 m, approximately 400 m below the paleosurface. This estimate is consistent with fluid-inclusion homogenization temperatures

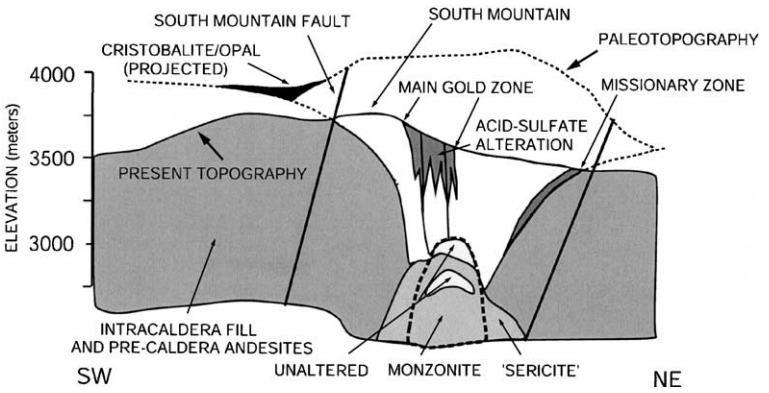

Fig. 3. Schematic NE–SW cross section of the Summitville mine area, showing pre-open-pit recent topography and reconstructed paleotopography, subvertical nature of acid-sulfate alteration and ore zones, and locations of underlying monzonite intrusion and sericitic alteration zone and cristobalite/opal sinter. The cristobalite/opal sinter is projected onto the plane of the cross section from approximately 1 km to the northwest. Displacement on South Mountain Fault removed. Modified from Steven and Ratté (1960) and Gray and Coolbaugh (1994).

discussed later. The cross section in Fig. 3, with displacements along the South Mountain and Missionary faults removed, illustrates the various geological relationships.

Isotopic dating indicates that emplacement of the South Mountain volcanic dome and both shallow acid-sulfate and deep phyllic alteration were closely related in time (Fig. 4). Getahun (1994) reported $^{40}Ar/^{39}Ar$ dates for biotite and sanidine from unaltered South Mountain quartz latite that are almost identical to earlier, less precise, K/Ar dates of Mehnert et al. (1973). Getahun's values for the South Mountain quartz latite overlap the upper end of the range of values for alunite, indicating that alteration closely followed emplacement of the South Mountain dome. Getahun (1994) also reported $^{40}Ar/^{39}Ar$ total-gas and plateau ages of 22.5±0.1 and 22.6±0.6 Ma, respectively, for 'sericite' from wallrock alteration related to pyrite–quartz stockwork veins in the quartz monzonite intrusion that underlies the district. Both the shallow acid-sulfate and deep quartz–'sericite' and kaolinite–pyrite alteration seem to have been part of the same hydrothermal system, but it cannot be determined whether they were coeval. It seems more likely that both the quartz–'sericite' and kaolinite–pyrite alteration antedate the shallow acid-sulfate alteration. Acid–sulfate alteration and mineralization proceeded through three hypogene stages and a supergene stage, punctuated by at least three periods of hydrothermal brecciation as distinguished by Gray and Coolbaugh (1994) and listed in Table 1.

Steven and Ratté (1960) first described the acid-sulfate alteration zonation at Summitville. The classic alteration zones grade outward from a core of intense acid leaching (vuggy silica) through a quartz–alunite zone to a quartz–kaolinite zone (which may be narrow

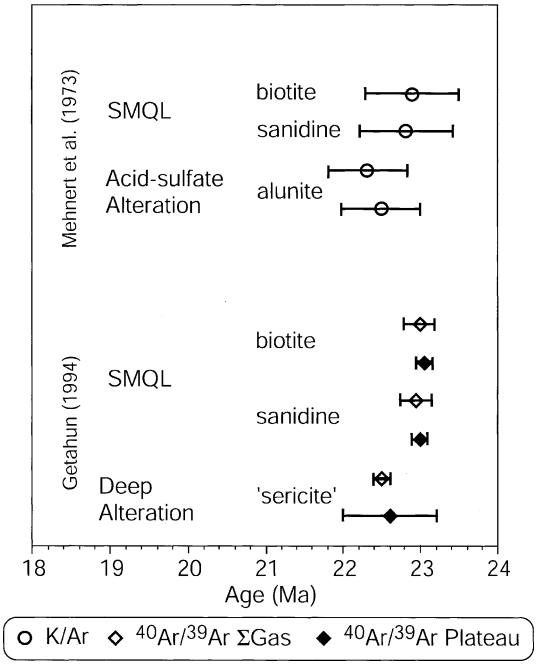

Fig. 4. Plot of radiometric age determinations by Mehnert et al. (1973) and Getahun (1994) for biotite, sanidine, and alunite from the South Mountain quartz latite (SMQL) and for deep alteration 'sericite'. Bars indicate reported uncertainties.

Table 1
Principal stages in the evolution of the Summitville hydrothermal system

Stage	Principal mineralogy
Acid-sulfate alteration and contemporaneous brecciation	Quartz, pyrite, alunite, kaolinite, illite, smectite
Main Stage Cu–Au–Ag mineralization	Quartz, pyrite, enargite, luzonite, covellite, native gold, kaolinite
Early hydrothermal brecciation	'Sericite', illite, pyrite
Late-stage base-metal–gold–barite mineralization	Barite, sphalerite, galena, pyrite, native gold, kaolinite
Kaolinite-matrix hydrothermal brecciation	Kaolinite
Supergene redistribution and alteration	Chalcocite, digenite, jarosite, goethite, native gold(?)

or absent) into an illitic zone. A distal smectite zone, rarely accompanied by carbonates, encloses the above sequence. All zones contain pyrite contemporaneous with alteration. The vuggy-silica zones are typically a few meters wide but can range up to 70 m across and be enclosed by an up to 30 m zone of strong quartz–alunite alteration. The acid-sulfate alteration zones narrow with depth, and most pass into quartz–'sericite'–pyrite zones at between 3400 and 3500 m (Stoffregen, 1987), although an alunite–pyrite pair was collected at an elevation of 2791 m. Small, local brecciation zones with angular to subangular clasts in an acid-sulfate-altered matrix were described by Gray and Coolbaugh (1994), who considered them to be contemporaneous with acid-sulfate alteration.

Main Stage mineralization was roughly coextensive with acid-sulfate alteration, but was most intense in the vuggy-silica zone. At the mined elevations, the ore assemblage consists of pyrite, enargite, luzonite, covellite, and gold or argentian gold, accompanied in places by sulfur and (or) marcasite (Stoffregen, 1987). Below approximately 3400 m elevation, the enargite±luzonite±covellite assemblage changes to one dominated by chalcopyrite+tennantite–tetrahedrite (Stoffregen, 1987), but enargite occurs sporadically down to an elevation of at least 2240 m. No samples of the chalcopyrite+tetrahedrite assemblage were analyzed in this study. Gold values are highest in the vuggy-silica zone and decrease outward until they fall below the recent mining cutoff grades of 0.34 $g \cdot t^{-1}$ outside the quartz–kaolinite zone.

Both acid-sulfate-altered and main-stage mineralized rock are cut by 'Early Hydrothermal Breccias' that include pebble dikes. The breccias and pebble dikes consist of heterolithic rounded to subrounded fragments in a clay-rich "rock flour" matrix of pyrite, 'sericite', illite, and minor alunite. Gray and Coolbaugh (1994) noted that clasts of quartz monzonite altered by quartz+'sericite'+pyrite indicate transport from deep in the hydrothermal system.

Late Stage veins of base metals+gold+barite containing up to 250 $g\ t^{-1}$ Au cut Early Hydrothermal Breccias and acid-sulfate-altered rocks. At lower mine levels, these veins contain pyrite, galena, sphalerite, barite, marcasite, kaolinite, and minor chalcopyrite with coatings of supergene chalcocite and fine-grained covellite (Gray and Coolbaugh, 1994). At higher levels, veins containing barite, goethite, jarosite, and gold or argentian gold were common according to Stoffregen (1987). Gray and Coolbaugh (1994) suggested that these oxidized veins, some of which contain visible gold and assay up to 4500 $g \cdot t^{-1}$ Au, are shallow expressions of the deeper base-metal–gold–barite veins and have been altered by supergene processes.

Scattered breccia pipes and dikes with a kaolinite matrix cut barite-bearing veins at several places and are the latest hydrothermal event at Summitville. These breccias contain fine-grained sulfides and Fe-oxide minerals of uncertain origin, and have high Au grades (Gray and Coolbaugh, 1994).

Supergene alteration, marked by the presence of goethite, jarosite, limonite, and hematite, is the final stage of mineral formation at Summitville. It penetrated deeply into the orebodies in the permeable vuggy-silica zone, but was limited to the upper 10 m or so in the surrounding zones (Gray and Coolbaugh, 1994). Narrow veins of fine-grained and apparently supergene alunite are present in the upper part of the deposit, but none was collected for this study. Copper was enriched substantially as expressed by fine-grained supergene chalcocite, digenite, and covellite. Some supergene enrichment of Au is probable, but the case is not as definitive as for Cu (Stoffregen, 1985, 1986, 1987).

3. Samples and analytical techniques

3.1. Sample locations and notation

Samples for analyses of fluid inclusions and stable isotopes were taken from outcrop, diamond-drill core,

dumps, and from mine benches. The coordinates and elevation, where known, are listed with the data for fluid inclusions and stable isotopes in Table 2 and Appendix A, respectively. Samples noted by hyphenated numbers were taken from diamond-drill core, the first number denoting the drillhole and the second the down-hole footage (uncorrected for plunge). The coordinates and elevations of the core samples are based on data for the surveyed location of the collar and the plunge and azimuth of the hole as supplied by

Table 2
Summary of fluid-inclusion data

Sample number	DDH core or surface	Mine area	Alteration zone	Northing[a]	Easting[a]	Elevation[a] (meters)	L>V or V>L	Th range (°C)	Number of inclusions	Salinity range, wt. % NaCl equiv.	Number of Inclusions
Secondary Fluid Inclusions in Phenocrysts											
300-672	DDH	Copper Hill	Vuggy Silica	51,494	100,441	3412	L>V	253–313	9	0.44–12.8	10
293-37	DDH	Tewksbury	Vuggy Silica	50,797	100,249	3648	L>V	175–295	64	0.53–18.0	7
DDH 5-1058	DDH	Annie	Vuggy Silica	52,857	99,717	3299	L>V	213–283	21	2.16–25.4	22
266-714	DDH	Hidden	Vuggy Silica	50,668	100,262	3433	L>V	223–258	17	2.82–6.4	13
320-1026	DDH	Hidden	Vuggy Silica	50,783	100,264	3357	L>V	167–260	31	0.97–16.2	33
322-655	DDH	Annie	Vuggy Silica	52,100	99,625	3425	L>V	169–305	18	0.27–1.99	18
323-744	DDH	Annie	Vuggy Silica	52,293	99,667	3390	L>V	177–295	19	0.79–12.5	18
323-742	DDH	Annie	Vuggy Silica	52,276	99,630	3390	L>V	207–285	10	1.82–24.7	12
281-401	DDH	Hidden	Quartz–Alunite	99,602	51,200	3552	L>V	201–241	22	1.82–4.42	24
266-359	DDH	Copper Hill	Quartz–Alunite	100,504	50,957	3522	L>V	215–254	10	1.82–7.80	18
25	Surface	Hidden	Vuggy Silica			3603	V>L	320–375	13		
26	Surface	Hidden	Vuggy Silica			3603	L>V	195–227	4		
14	Surface	Annie	Quartz–Alunite			3612	L>V	192–262	17	1.48–5.41	27
27	Surface	Hidden	Illite/Kaolinite			3603	L>V	135–232	9		
82	Surface	Copper Hill	Illite			3523	L>V	214–373	18	2.32–4.57	14
83	Surface	Copper Hill	Illite			3523	L>V	219–347	8	2.24–5.11	5
							V>L	337–347	4		
84	Surface	Copper Hill	Illite			3523	L>V	211–251	10	3.87–3.95	7
30	Surface	Hidden	Smectite			3603	L>V	183–214	19		
32	Surface	Hidden	Smectite			3603	L>V	327–354	7	5.64–5.94	2
92	Surface	Copper Hill	Smectite			3517	L>V	249–389	7	8.28	1
Main Mineralization Stage Quartz											
DDH5-288	DDH	Annie	N/A	99,717	52,857	3533	L>V	203–367	21		
SV79-1	Surface (Dump)	Missionary	N/A	*100,500*	*53,400*	*3444*	L>V	197–383	133	32.4–34.5	4
							V>L	263–387	7		
Deep Pyrite–Quartz Stockwork											
DDH-14-3498	DDH	Iowa	N/A	100,876	50,502	2540	L>V	223–497	64	35.1–42.3	8
						2540	V>L	323–473[b]	7		
DDH-14-4734	DDH	Iowa	N/A	100,876	50,502	2163	L>V	297–387	2		
							V>L	373–463[b]	3		

[a] Numbers in italics are estimated values (see text).
[b] Many inclusion homogenized to vapor above 500 °C.

Summitville Consolidated Mining (M. Coolbaugh, written communication, 1991), and on logged core footages corrected for the azimuth and declination of the drillhole. The coordinates of surface and dump samples are known less well. Their elevations are constrained within a few meters, but the uncertainties in their northing and easting coordinates may be substantial. If their approximate coordinates (±20 m) are known, they are noted in italics in Table 2 and Appendix A. Otherwise, no entry is listed.

3.2. Analytical techniques

Quartz, kaolinite, pyrite, and water in fluid inclusions were analyzed for isotopic compositions by standard techniques using conventional stable-isotope analyses. Alunite was separated and prepared for isotopic analysis of H, O, and S sites in alunite using the methods of Wasserman et al. (1992). Sulfide sulfur was extracted from chalcopyrite included in biotite and magnetite by using a modification of the chromic ion technique described by Tuttle et al. (1986), and was analyzed as Ag_2S using standard techniques. Sulfate sulfur in apatite was extracted by Kiba reagent (Ueda and Sakai, 1984) and was analyzed as Ag_2S by the same standard techniques.

Thermometric data on fluid inclusions were obtained using a USGS design gas-flow heating–cooling stage. Precision of heating measurements was ±5 °C, and was ±0.5 °C for measurements of freezing-point depression.

4. Fluid-inclusion evidence

4.1. Fluid-inclusion microthermometry samples

Thermometric data were obtained on secondary fluid inclusions along healed fractures in quartz phenocrysts in the South Mountain quartz latite from each of the four alteration zones. Data were also obtained on inclusions in vein quartz from the Missionary dump and from deep exploration drillholes DDH-5 and DDH-14. Measurements of homogenization temperature were made on 574 inclusions from 24 samples. The temperature estimates have not been corrected for pressure. Salinity (NaCl equivalent) estimates were made on 243 inclusions from 18 samples. Homogenization temperature and salinity ranges are summarized in Table 2, and the complete data set is available in Stoffregen et al. (2004).

The results of several previous fluid-inclusion studies of Summitville samples have been published. Bruha and Noble (1983) reported a range of homogenization temperatures of 231 to 276 °C and a salinity range of 7 to 21 wt.% NaCl equivalent for an unspecified number of secondary inclusions in quartz phenocrysts from Summitville. They also reported the presence of as many as five daughter minerals in inclusions from Summitville quartz. Cunningham (1985) reported visually estimated trapping temperatures of approximately 100 °C for fluid inclusions in barite from the famous Summitville Boulder. Stoffregen (1985) reported homogenization temperatures of 230–320 °C and salinities of 3.2 to 5.3 wt.% NaCl equivalent for primary inclusions in drusy quartz crystals lining vugs and intergrown with sulfide minerals in the vuggy-silica zone.

4.2. Fluid inclusions from the main alteration–mineralization zone

4.2.1. Secondary fluid inclusions in quartz phenocrysts

Homogenization and freezing temperatures were measured on fluid inclusions trapped along fractures in quartz phenocrysts in the South Mountain quartz latite from the Annie, Copper Hill, and Hidden/Tewksbury areas (Table 2, Fig. 2). The vuggy-silica, quartz–alunite, illite, and smectite alteration zones were sampled. In all samples, the phenocrysts contained numerous intersecting healed fractures. In most cases, the data for each locality were obtained on a single phenocryst. In many phenocrysts, inclusions from several areas were measured. An attempt was made to confine sets of measurements to individual planes. However, because of the complexity of the fracture networks, some of the inclusions considered to be along a given plane may have been trapped along an intersecting plane. It is also possible that some inclusions along a given plane may have been reopened by a later fracture and their fluids replaced by or mixed with later fluids (cf. Foley et al., 1990). It was not possible to determine, by petrographic means, either the relative timing of trapping between planes or the relationship of trapping to the evolution of the

Summitville hydrothermal system. As a whole, the data represent time-integrated samples of the fluids involved in the system. Nevertheless, some important observations and speculations can be made from the data for secondary fluid inclusions as discussed below.

Inclusions along most planes homogenized to a liquid phase (liquid-rich inclusions). However, those along a few planes homogenized to vapor (vapor-rich inclusions). A number of planes of inclusions with large vapor bubbles were seen but not measured because of the difficulty in determining temperatures of homogenization to vapor on small inclusions. Thus, vapor-rich inclusions are much more abundant than they appear to be from Table 2.

Fig. 5a is a stacked histogram of homogenization temperatures for all liquid-rich secondary inclusions from the three mine areas. Fig. 5b–d shows the temperature distribution of each alteration zone by mine area. Measured temperatures for liquid-rich inclusions fall into two groups: a low-temperature group that homogenized between approximately 170

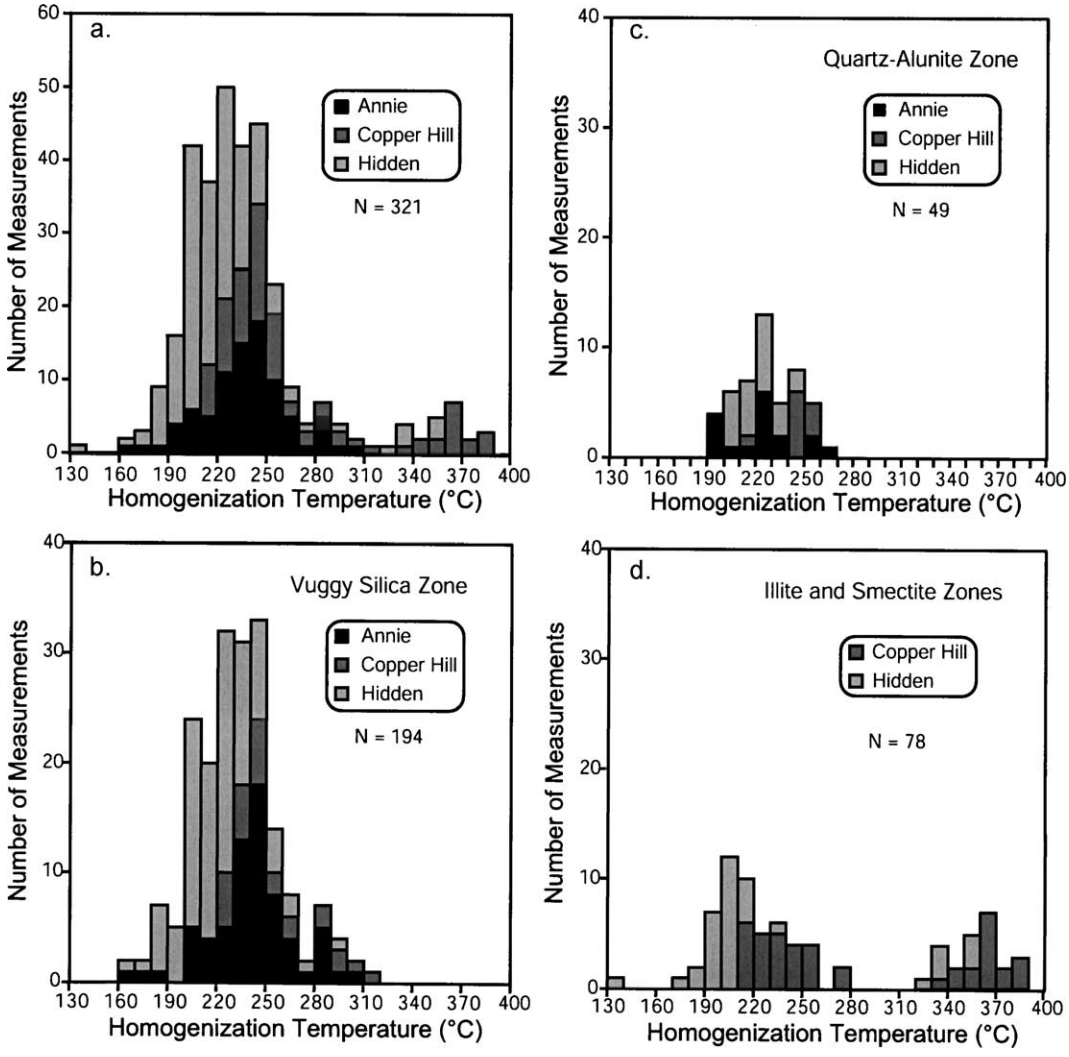

Fig. 5. Stacked histograms of homogenization temperatures of liquid-rich secondary fluid inclusions in quartz phenocrysts from the main mineralized zone. (a) Data from all alteration zones by mine area. (b–d) Data for each alteration zone by mine area. Note change in frequency scale between (a) and (b–d).

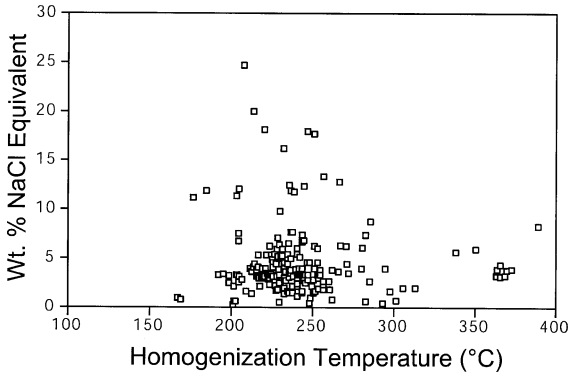

Fig. 6. Plot of homogenization temperature vs. salinity (NaCl equivalent) for individual liquid-rich secondary fluid inclusions in quartz phenocrysts. Data are for all mine areas and alteration zones in the main mineralized zone.

and 280 °C, and a much smaller high-temperature group that homogenized between approximately 320 and 390 °C. Only 13 of the 337 inclusions homogenized at temperatures intermediate between the two groups. Inclusions in the high-temperature group occur only in the illite and smectite zones (which were not sampled at the Annie mine area). The temperatures for the high-temperature group are higher than the upper stability limit of kaolinite and smectite, indicating that the inclusions were trapped prior to wallrock alteration, and probably are unrelated to the Summitville hydrothermal system. More likely, the inclusions represent deuteric fluids trapped at lithostatic pressures at depth during the growth of the South Mountain dome.

Vapor-rich inclusions, which occurred along planes containing only vapor-rich inclusions, were measured in one sample each from the vuggy-silica and illite zones where they occurred. The inclusions homogenized to vapor over a narrow range (~10 °C) between 320 and 368 °C, roughly the same interval as that for the high-temperature group of liquid-rich inclusions. A few samples (notably 82 and 92, from the illite and smectite zones in the Copper Hill area) had numerous vapor-rich inclusions along planes of mainly liquid-rich inclusions, but homogenization temperatures were not measured. It seems probable that the vapor-rich inclusions were trapped along with the high-temperature liquid-rich inclusions and represent deuteric fluids trapped under lithostatic pressure but at depths shallow enough that the deuteric fluids boiled.

Measurements of freezing-point depression were made on 243 secondary inclusions (Stoffregen et al., 2004). Salinities were calculated using the equations of Bodnar (1993), ignoring the possible presence of CO_2. Fig. 6 is a plot of salinity vs. homogenization temperature for inclusions on which both were measured. Most of the values cluster between 200 and 275 °C and 0–5 wt.% NaCl equivalent, but salinities extend to 25 wt.% and temperatures to 320 °C. There appears to be no systematic relationship between temperature and salinity.

Fig. 7 shows values of NaCl equivalent for the four alteration zones. Most of the inclusions (76%) have salinities less than 5 wt.% NaCl equivalent, with a strong mode at 4 wt.%. Inclusions with salinities above 5 wt.% occur almost exclusively in the vuggy-silica zone (two inclusions with a salinity of 7.8 wt.% NaCl equivalent occur in the quartz–alunite zone). The vuggy-silica zone hosts the vast majority of the main-stage Cu–Au mineralization, suggesting that the metals were transported by the higher-salinity fluids, a suggestion supported by fluid-inclusion data on quartz intergrown with ore minerals in samples collected from the Missionary vein dump, discussed below.

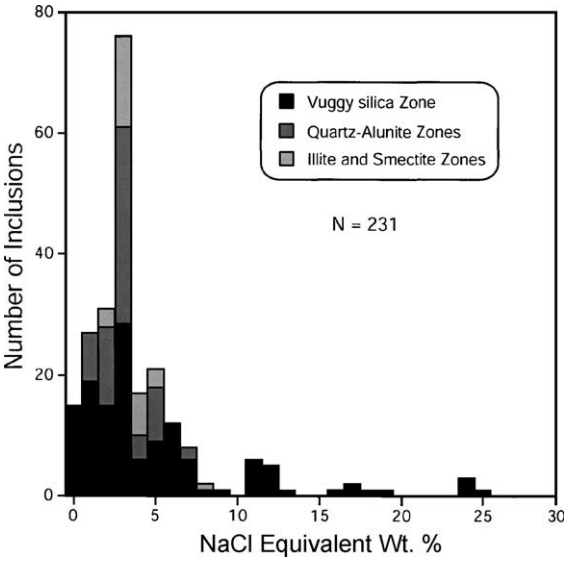

Fig. 7. Histogram of salinities (NaCl equivalent) for liquid-rich secondary fluid inclusions in quartz phenocrysts from the main mineralized zone.

4.2.2. Variability of liquid/vapor ratio, homogenization temperature, and salinity in secondary inclusions

Most phenocrysts contain either liquid-rich or vapor-rich inclusions, but some contain both types. Some apparent planes were seen to contain both liquid- and vapor-rich inclusions, but the vapor-rich inclusions were not used, as noted above. The presence of both liquid- and vapor-rich inclusions along healed fractures in the quartz phenocrysts indicates that mixed-phase inclusions were trapped at times.

Inclusions that homogenize to liquid varied considerably in homogenization temperature, salinity, or both, within each phenocryst and within individual areas of many phenocrysts. Some of the variation in homogenization temperature (and, possibly, homogenization phase) is likely due to necking down of inclusions during healing, but large salinity variations cannot be due to this process. Consequently, most of the variation is attributed to trapping of disparate fluids during the evolution of the system. Although it was not possible to develop even an approximate time sequence from the observed features, the data do demonstrate that at various times over the life of the hydrothermal system, the main mineralization–alteration zone was occupied by both low-density and condensed and aqueous fluids at various temperatures; these fluids had both high salinities and low to moderate salinities.

4.2.3. Fluid inclusions from deep pyrite–quartz stockwork veins

Homogenization temperatures were measured on presumed primary fluid-inclusions in vein quartz from DDH-14 intercepts at elevations of 2536 m (DDH-14-3498) and 2160 m (DDH-14-4734). The most robust data set is from DDH-14-3498, wherein 64 of 71 inclusions homogenized to liquid, the remaining seven to vapor. A halite daughter mineral occurred in eight of the inclusions that homogenized to liquid. The large range of homogenization temperatures in Fig. 8a has

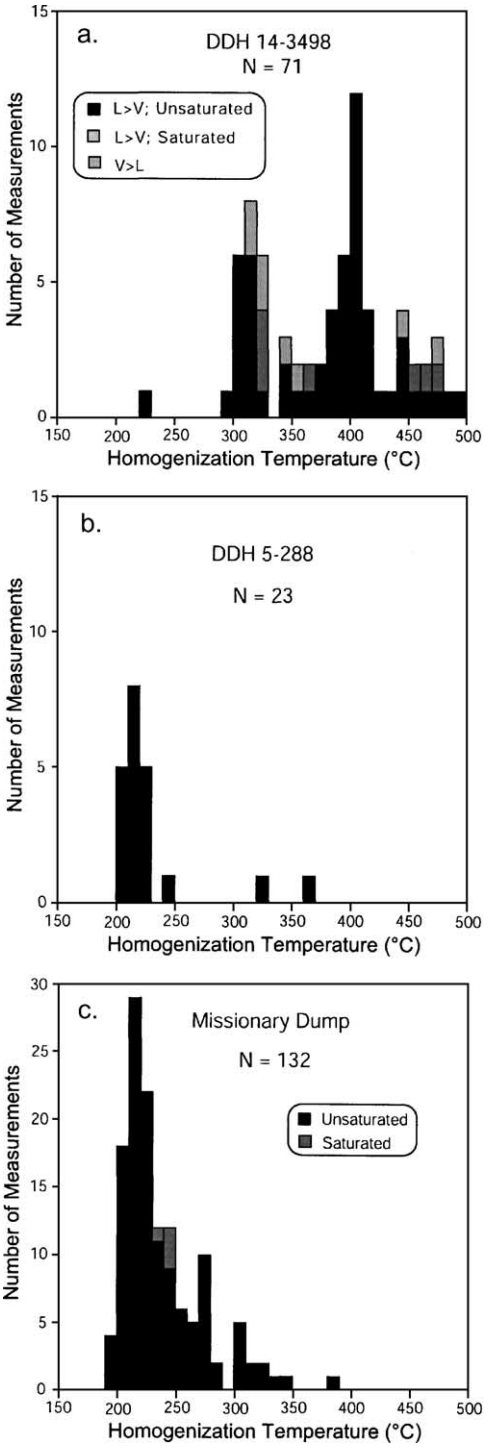

Fig. 8. Stacked histograms of homogenization temperatures of fluid inclusions from vein quartz from the main mineralized zone and deep pyrite–quartz stockwork zone. (a) Vapor-rich and saturated and unsaturated liquid-rich inclusions from deep stockwork vein (2545 m elevation). (b) Unsaturated liquid-rich inclusions from sample DDH5-288 (3533 m elevation). (c) Saturated and unsaturated liquid-rich inclusions from the Missionary vein (dump sample, ~3444 m elevation).

two modes, one about 310 °C, the other around 400 °C. In addition to the temperatures reported, numerous inclusions homogenized to vapor at temperatures >500 °C, the limit of measurement. The simplest interpretation of the data for DDH-14-3498 is that they record a time-integrated sample of both liquid and vapor trapped over a range of temperatures at various times during vein filling.

The temperature of dissolution of the halite daughters ranged from 269 to 354 °C, indicating an approximate salinity range of 35 to 42 wt.% NaCl equivalent for the saturated inclusions based on the H_2O–NaCl binary (Sourirajan and Kennedy, 1962). No measurements of freezing-point depression were made on the unsaturated inclusion fluids, so the overall range of salinities is not known. The high salinities estimated from the disappearance of the daughter minerals document the presence of concentrated brines at depth.

Only five inclusions were measured from sample DDH-14-4734. Two homogenized to liquid at 297 and 288 °C, respectively, and three to vapor, one at 272 °C and two at 362 °C. The vast majority of the inclusions, both liquid- and vapor-rich, homogenized at temperatures above 500 °C. No measurements of freezing-point depression were attempted on this sample.

4.2.4. Inclusions in vein quartz from drillhole DDH-5

Homogenization temperatures were measured on 21 presumed primary fluid inclusions in vein quartz from ASARCO diamond drillhole DDH-5 at an elevation of 3609 m (Sample 5-288). The timing of the vein relative to the evolution of the hydrothermal system is not known with certainty, but the presence of enargite–luzonite and pyrite with vein quartz in adjacent samples suggests that the inclusions represent main-stage ore fluids. All inclusions homogenized to liquid, all but two of them between 200 and 245 °C (Fig. 8b). No measurements of freezing-point depression were made on this sample.

4.2.5. Ore-stage inclusions in quartz, Missionary vein area

A dump sample of coarsely crystalline quartz intergrown with enargite–luzonite, pyrite, and gold was collected from the Missionary vein area. Homogenization temperatures of presumed primary inclusions range from 198 to 387 °C (Fig. 8c). Most inclusions homogenized to liquid, but several homogenized to vapor. Four of the inclusions contained a halite daughter mineral. Ninety-five percent of the liquid-rich inclusions homogenized at <315 °C, including all four inclusions containing a halite daughter. Pairs of adjacent inclusions homogenizing to liquid and vapor did so at 260–270, 310–320, and 380–390 °C (two pairs). If these measurements on liquid- and vapor-rich pairs represent boiling, an improbable range of pressure and salinity is implied. These values more likely reflect the presence of noncoeval inclusions or the necking down of inclusions during healing of a fracture. Salinities of 30–35 wt.% NaCl equivalent, estimated from the H_2O–NaCl binary data of Sourirajan and Kennedy (1962), are implied for inclusions containing halite daughters.

4.2.6. Inclusions in barite from the Summitville Boulder

Cunningham (1985) visually estimated homogenization temperatures of ~100 °C in barite from the Summitville Boulder, which is on display at the Denver Museum of Natural History. The boulder was discovered on a road in the upper part of the deposit, and presumably came from a location above the road. Because of the susceptibility of barite to postdepositional leakage of inclusions, homogenization temperatures measured on barite from the boulder in this study (which ranged from 190 to 389 °C) are not considered reliable, and no measurements have been made on any other barite from Summitville.

4.3. Summary and interpretation of fluid-inclusion studies

Despite the lack of clear paragenetic control, important interpretations, even if speculative, can be made on the basis of the fluid-inclusion data. The homogenization temperature range of the vast majority of the fluid inclusions in both the main zone of mineralization–alteration and the deep stockwork is consistent with the temperatures determined from the sulfur-isotope fractionation between alunite and pyrite, thus adding credibility to both estimates. The occurrence of inclusions that homogenize both to vapor and liquid indicates that a low-density phase was present at some time or times and at all levels of the system.

The salinities of the inclusion fluids fall into two overlapping groups: (1) low to moderate salinity with NaCl equivalents of <5 wt.%, and (2) high salinity with up to 42 wt.% NaCl equivalent. The high-salinity inclusions on healed fractures in quartz phenocrysts are mainly confined to the vuggy-silica zone, as was most of the Cu–Au mineralization. Inclusions in vein quartz associated with enargite and gold in sample from 5-288 and from the Missionary dump also contain high-salinity fluids and homogenize over a similar temperature range. These observations strongly suggest that the high-salinity fluids were responsible for the main-stage mineralization. The fluids of low to moderate salinity found in secondary inclusions in quartz phenocrysts in all alteration zones likely derived part of their salinity through the intense leaching of the wallrocks by sulfuric acid that was generated by the disproportionation of SO_2, and by HCl. Therefore, the resulting fluids are likely to have been mixtures of aqueous Na, K, and Al sulfates and chlorides and, possibly, residual H_2SO_4.

Fluid-inclusion homogenization temperatures are plotted as a function of elevation in Fig. 9. Boiling-point curves for 5% and 25% NaCl brines under both lithostatic and hydrostatic pressure regimes are plotted for reference. The lithostatic curves are arbitrarily anchored at the elevation of the top of the South Mountain dome (~4150 m) as reconstructed by Steven and Ratté (1960). The hydrostatic curves are anchored 150 m lower, reflecting a reasonable estimate of the maximum depth to the water table. Most of the homogenization temperatures on liquid-rich inclusions from the main zone of alteration–mineralization plot below the 5% hydrostatic curve. Notably, nearly all inclusions in the high-salinity group (>5% NaCl equivalent) also plot on or below the 5% hydrostatic boiling curve (Fig. 10). This fact and the extremely high salinity of some inclusions imply that they did not achieve their high salinity by boiling of the low-salinity fluids, and must have a different origin. A few inclusions that homogenized to liquid of moderate salinity (~6 wt.%) plot near or above the lithostatic

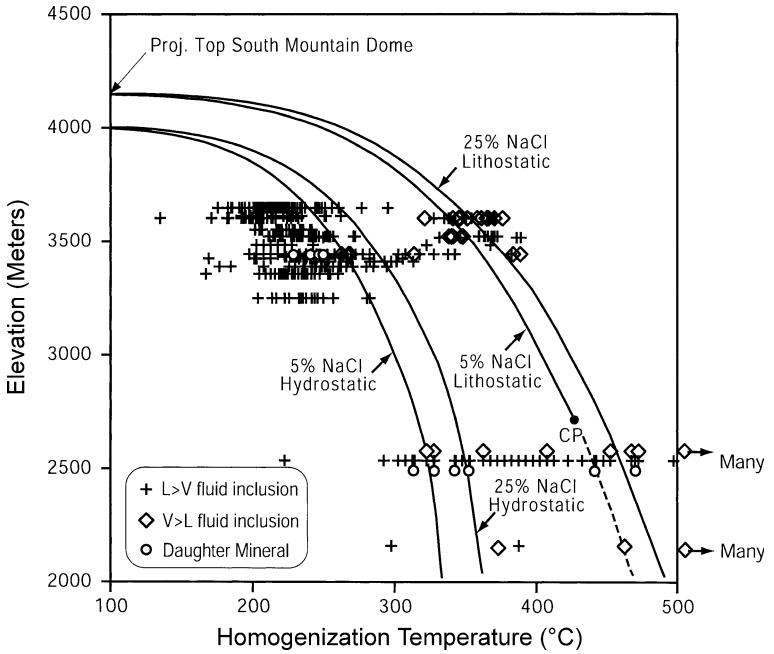

Fig. 9. Plot of homogenization temperatures of fluid inclusions vs. present elevation. Boiling-point curves for 5 and 25 wt.% NaCl for both hydrostatic and lithostatic hydrologic regimes are plotted for reference (data from Haas, 1976; Sourirajan and Kennedy, 1962). Projected elevation of top of South Mountain Dome from Steven and Ratté (1960). L>V=inclusion homogenized to liquid. V>L=inclusion homogenized to vapor. CP=critical point. Points for daughter minerals and vapor-rich inclusions are offset from true 2540 m elevation for clarity. Note that many inclusions in quartz veins deep in the system homogenized to vapor at temperatures >500 °C.

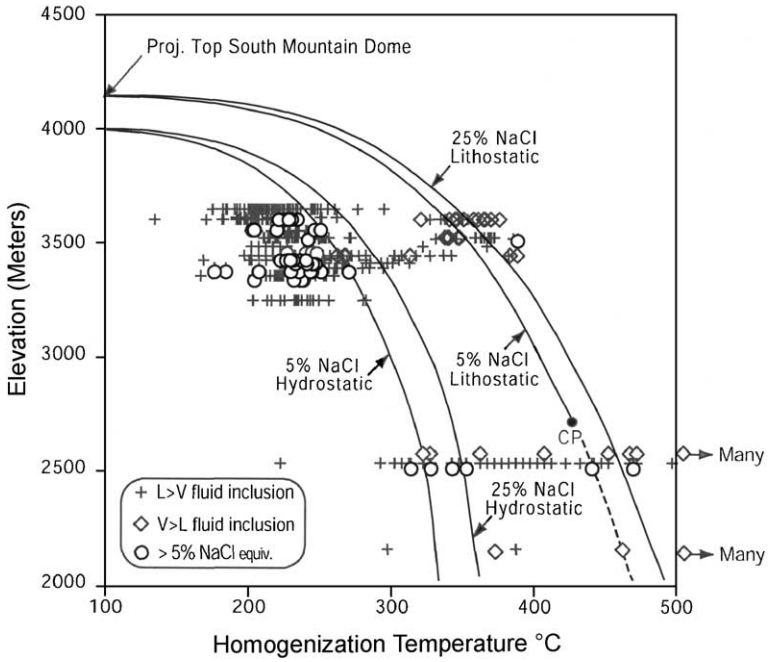

Fig. 10. Plot of homogenization temperatures of fluid inclusions with salinities greater than 5 wt.% NaCl equivalent superimposed on those in Fig. 9 (shaded symbols). Notation as in Fig. 9.

curves at elevations greater than 3500 m, as do all inclusions from this depth range that homogenized to vapor. As noted above, these inclusions are interpreted to have trapped deuteric fluids generated during crystallization of the South Mountain quartz latite deep in the system during the growth of the dome.

Homogenization temperatures for both liquid-rich and vapor-rich inclusions in stockwork quartz from 2536 m elevation have temperatures that span the range between the hydrostatic and lithostatic sets of boiling curves (Fig. 9). Daughter minerals were noted in several of the inclusions whose melting temperatures indicated salinities up to 42 wt.% NaCl equivalent. The sample also contained numerous inclusions that homogenized to vapor at >500 °C. These ranges in homogenization temperature, salinity, and liquid–vapor ratio suggest trapping of a mixed liquid–vapor fluid, as described by Bodnar et al. (1985) for synthetic fluid inclusions in their experimental study of the system H_2O–NaCl. The inclusions undoubtedly represent a time-integrated sample of the mother fluid(s), and part of the ranges may be due to variations in the fluid attributes with time. Stockwork quartz from an elevation of 2160 m contained inclusions that homogenized to either liquid or vapor, mainly at >500 °C, but two pairs homogenized to both liquid and vapor at temperatures of about 360 and 460 °C, indicating trapping of a two-phase fluid at some time.

5. Stable-isotope evidence

The low-pH environment during acid-sulfate alteration at Summitville is conducive to the attainment of isotope equilibrium among all aqueous species in the hydrothermal fluids and between aqueous species and minerals (Ohmoto and Lasaga, 1982; Rye, this issue). The sulfur-isotope fractionations between coexisting sulfide and sulfate minerals and the oxygen-isotope fractionation between quartz and alunite as well as between the sulfate and OH sites in alunite, provide potential geothermometers. The presence of hydrous minerals both in alteration and in vein-filling stages at Summitville facilitates the identification of sources and evolution of fluids. The stable-isotope analytical data and fluid compositions calculated from the minerals are summarized in Appendix A.

5.1. Stable-isotope geothermometry

5.1.1. South Mountain quartz latite

Apatite needles up to 1 cm in length are abundant in the groundmass of the South Mountain quartz latite porphyry. They also occur as clots in the cores of K-feldspar phenocrysts. Apatite containing sulfate sulfur up to 1300 g t^{-1} was concentrated by heavy-liquid separation for $\delta^{34}S$ analysis of sulfate. Sulfate sulfur in apatite has a $\delta^{34}S$ value of 5.5‰. Hand-picked biotite and magnetite phenocrysts contain rare, 2 to 20 μm inclusions of chalcopyrite that yielded $\delta^{34}S$ values of −2.3‰ and −6.3‰, respectively. The sulfur-isotope fractionations between sulfate in apatite and the chalcopyrite in biotite and magnetite correspond to temperatures of 485 and 670 °C, respectively. As discussed below, the oxygen-isotope fractionation between quartz and biotite phenocrysts indicates that the temperature of crystallization of the quartz latite was probably close to 780 °C. Solid-state reaction rates in chalcopyrite are among the fastest of the common sulfide minerals (Barton and Skinner, 1979). The apparently low sulfur-isotope temperatures most likely reflect continued chalcopyrite exchange with magmatic sulfur as the South Mountain porphyry cooled; thus, the oxygen-isotope quartz-biotite fractionation temperature is considered to be a better estimate of the temperature of crystallization of the porphyry. Accordingly, an "adjusted" $\delta^{34}S$ value for chalcopyrite of −0.3‰ was calculated for a temperature of 780 °C using the fractionation factors of Ohmoto and Lasaga (1982) and is considered a better approximation to the original value for chalcopyrite in the phenocrysts in the porphyry.

It is also possible that the sulfur-isotope fractionations between apatite and chalcopyrite reflect changes in the bulk $\delta^{34}S$ of the magma with time during crystallization. Such changes could be due to evolution of a volatile phase or to assimilation of sulfur-bearing wallrocks. Neither is likely to have been the case at Summitville. Apatite and phenocrystic magnetite and biotite, and presumably their contained chalcopyrite, formed early in the crystallization history of the magma prior to the concentration and release of volatiles as a consequence of the crystallization of anhydrous minerals. Assimilation of sulfur-bearing wallrocks with significantly different bulk ^{34}S values during crystallization is similarly unlikely considering the small size, eruptive history, and volcanic setting of the South Mountain porphyry.

5.1.2. Acid-sulfate alteration

Isotopic data for sulfide–sulfate pairs and individual sulfide minerals are presented in Appendix A along with calculated sulfide–sulfate isotopic temperatures for coexisting mineral pairs. Estimated temperatures decrease from 780 °C for samples interpreted to have formed during crystallization of the host quartz latite porphyry, through 390° for a sample of altered quartz monzonite at depth in the system, to between 250 and 200 °C within the main orebody. The temperatures calculated from the sulfur-isotope fractionation between pyrite and alunite are consistent with homogenization temperatures of fluid inclusions in quartz phenocrysts, as illustrated in Fig. 11. As do the majority of the fluid-inclusion homogenization temperatures, the temperatures estimated from the pyrite–alunite sulfur isotope fractionation on samples from the main mineralized zone fall below the hydrostatic boiling curve for a fluid of 5 wt.% NaCl equivalent. The pyrite–alunite estimated temperature for the deep sample, however, falls closer to the lithostatic boiling curves and is taken to indicate equilibration at a depth close to the lithostatic–hydrostatic transition.

Other potential stable-isotope geothermometers involving the fractionation of oxygen isotopes between the SO_4 and OH sites in alunite and between alunite and quartz were evaluated and found not to be useful for Summitville (Rye et al., 1990). Measured oxygen-isotope fractionations between the SO_4 and OH sites in alunite at Summitville are small and lead to calculated temperatures of 305–502 °C, substantially higher than those estimated from the sulfur-isotope fractionation between pyrite and alunite and those estimated from fluid-inclusion homogenization measurements. The measured $\Delta^{18}O_{SO4}$–$^{18}O_{OH}$ fractionations apparently are not equilibrium values. Rye et al. (1990, 1992) interpreted this departure of $\Delta^{18}O_{SO4–OH}$ from equilibrium to result from retrograde exchange between the OH site and later fluids. Support for this possibility is that the δD values of some samples suggest that some alunite underwent retrograde exchange with later fluids, as is discussed later. Alternatively, but less probably, the departure may be an artifact of the analytical procedure wherein

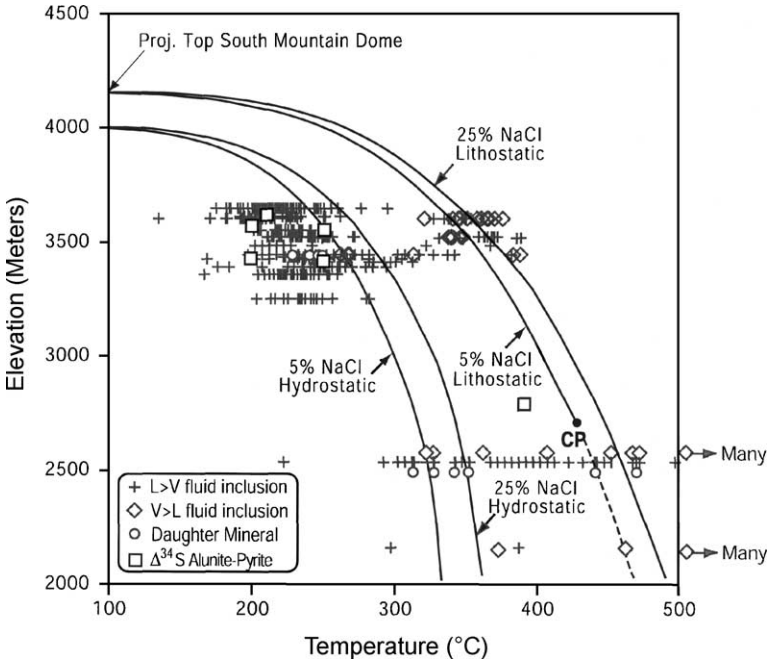

Fig. 11. Plot of pyrite–alunite $\delta^{34}S$ fractionation temperature estimates vs. elevation superimposed on fluid-inclusion homogenization temperature data from Fig. 9 (shaded symbols). Notation as in Fig. 9.

the $\delta^{18}O$ value for the OH site is determined by difference between that for the whole mineral and that for the SO_4 site (Wasserman et al., 1992). Minor errors in the analysis or small amounts of impurities can lead to large percentage departures from equilibrium $\Delta^{18}O_{SO4-OH}$ values, which at temperatures of 200 to 400 °C are only 4.6‰ to 2.8‰, respectively. Only for the 1.8 Ga alunite at Tapajós, Brazil, does this intramineral thermometer seem to work reasonably well for a high-sulfidation deposit (Juliani et al., this issue). The oxygen isotope fractionations between quartz and either the SO_4 or OH sites in alunite do not seem to be useful indicators of temperature of deposition. The fractionation between quartz and the SO_4 site is too insensitive to temperature to give meaningful temperature estimates (Rye et al., 1990), and although the fractionation between quartz and the OH site is sensitive enough to temperature to be a geothermometer, the observed fractionations are much too small and give an unreasonable range of temperatures (11–727 °C). Thus, the $\Delta^{18}O_{quartz-alunite(OH)}$ geothermometer fails at Summitville for the same reasons as did the $\Delta^{18}O_{SO4-OH}$ intramineral thermometer.

5.1.3. Main Stage and late barite and base-metal mineralization

Unlike in the Acid-Sulfate Alteration Stage at Summitville, sulfate minerals were not deposited during Main Stage Cu–Au–Ag mineralization. Therefore, sulfide–sulfate geothermometry can be used only to estimate temperatures of the relatively minor late-stage barite+sphalerite+galena veins that occur locally within the deposit. One barite–sphalerite pair from the Annie split area (Fig. 2) in the deeper part of the ore zone (ROR-SV-2-89) yielded a reasonable value of 214 °C. This estimate may be fortuitous, however, as it may not represent an equilibrium temperature because sulfur-isotope exchange between aqueous sulfate and sulfide is kinetically inhibited in the more neutral and lower temperature solutions typical of barite deposition (Ohmoto and Lasaga, 1982).

5.2. Sources and evolution of fluids

In all types of volcanic-hosted epithermal deposits, end-member fluids from two primary sources are typically involved: magmatic and meteoric. The isotopic compositions of each may evolve through

reaction with wallrock or by mixing with one another. It is necessary to estimate the original composition of each to trace such fluid evolutionary paths.

5.2.1. Composition of magmatic and meteoric water

The isotopic composition of aqueous fluids generated during the crystallization of a magma body underlying Summitville may be estimated from that of unaltered samples of the South Mountain quartz latite porphyry, assuming it to be representative of the source magma. Whole-rock samples of fresh South Mountain quartz latite (samples 735-1349a–b in Appendix A) have $\delta^{18}O$ values of 7.3–7.8‰, typical of I-type felsic igneous rocks (O'Neil and Chappell, 1977). A similarly unaltered sample (Summ SM-1) yielded $\delta^{18}O$ values of 9.4‰ for quartz, 8.5‰ for K-feldspar, and 6.7‰ for biotite phenocrysts. The δD value of biotite is −90‰, attesting to the lack of significant postcrystallization alteration. Using the fractionation factors of Bottinga and Javoy (1973), the quartz–biotite oxygen isotopic fractionation gives a temperature of 780 °C, whereas the much less temperature-sensitive quartz–K-feldspar $\delta^{18}O$ fractionation gives a temperature of 765 °C. The quartz–water, feldspar–water, and biotite–water fractionations all give values of $\delta^{18}O_{H2O}$ of 9.4. These remarkably concordant and realistic temperatures and $\delta^{18}O_{H2O}$ values confirm the pristine nature of the sample of quartz latite. Therefore, the isotopic composition of the minerals can be used to estimate the composition of primary magmatic fluids in equilibrium with the underlying magma.

The boxes for primary magmatic water (PMW; Taylor, 1979), and felsic magmatic water (FMW; Taylor, 1992) in Fig. 12 are conventional references, as are the meteoric water and kaolinite lines. The compositions of magmatic waters from a given area may fall outside these boxes, and waters of other origins may have compositions that fall within them. The δD and $\delta^{18}O$ of water in the primary fluids separated at 780 °C from the source magma at Summitville, estimated from the isotopic composition of unaltered biotite in the South Mountain quartz latite, are −68‰ and 9.4‰, respectively (Fig. 12). Wherever exsolved during crystallization, these fluids migrated upward into the plastic subsolidus region of the carapace of the intrusion, remaining there until release into the surrounding hydrostatically pressured brittle fracture zone (Burnham, 1979; Fournier, 1992). In so doing, the fluids underwent isotopic exchange with the crystallizing magma and ductile portion of the carapace at successively lower submagmatic temperatures and at very low water–rock ratios. Both values decreased substantially, as is shown by the series of diamonds along the calculated magmatic fluid exchange track in Fig. 12 (Ohmoto and Rye, 1974; Rye, 1993). It is useful to identify these deep fluids, whose isotopic composition was modified by isotopic exchange in the carapace and upper parts of the magma chamber, as *evolved* magmatic fluids in order to distinguish them from the *primary* magmatic fluids as they were when released from the magma chamber. That this deep isotopic exchange took place at Summitville is strongly indicated by the proximity of the calculated fluid composition for the deep alunite sample to the end of the exchange track, and the previously noted position of that sample near the brittle–ductile transition. Such an exchange process should be expected in other epizonal intrusions if, as commonly assumed, the exsolved fluids accumulate beneath the brittle–ductile transition and within the carapace prior to release into the superjacent fracture system.

Taylor (1974) inferred a δD value of −80‰ and a $\delta^{18}O$ value of −11‰ for meteoric water in the eastern San Juan volcanic field on the basis of data from the 29.1 Ma Alamosa River stock, which intruded the center of the Platoro caldera roughly 5 km south of the Summitville deposit. Present-day meteoric water in the area has values of $\delta D = -118‰$ to −105‰, and $\delta^{18}O = -16.0‰$ to −14.5 ‰. Our δD values for the late-stage kaolinite of the Summitville deposit indicate that meteoric water in the area had a δD as low as −115‰ at the time of mineralization at 22–21 Ma. Values of $\delta D = -110 \pm 10‰$ and $\delta^{18}O = -15.0 \pm 2‰$ are adopted for this discussion.

5.2.2. Acid-sulfate alteration fluids

The isotopic composition of water in fluids responsible for quartz–alunite alteration at Summitville can be calculated from alunite δD and $\delta^{18}O$ values using the fractionations determined experimentally by Stoffregen et al. (1994). Because the sulfate site is more reliable than the hydroxyl site for the retention of primary oxygen-isotope compositions in alunite, $\delta^{18}O_{SO4}$ was used in these calculations.

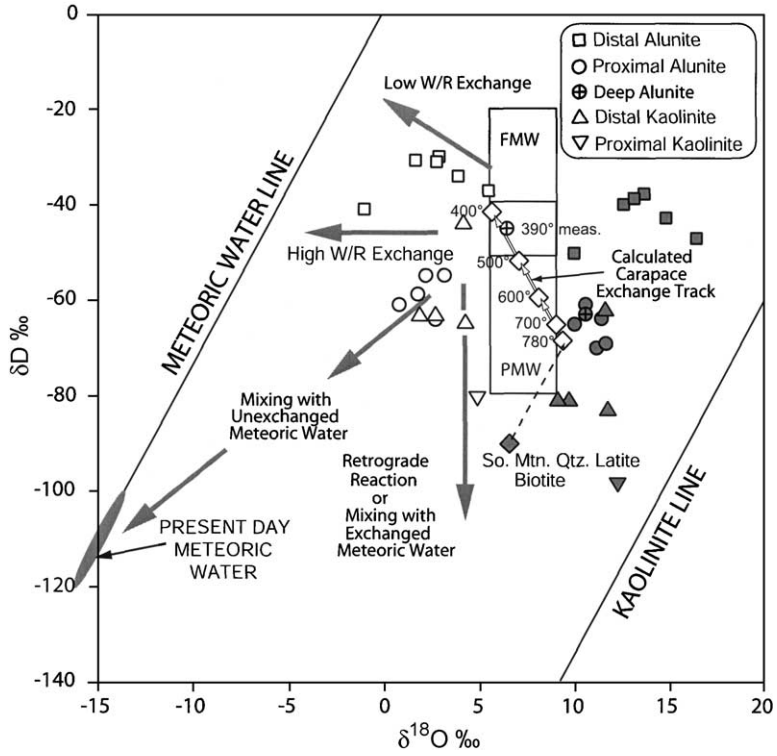

Fig. 12. Plot of $\delta^{18}O$ vs. δD values for acid-sulfate alteration alunite and kaolinite and biotite from the South Mountain porphyry (solid symbols) and fluids calculated from the mineral data (open symbols). Temperatures used for fluid calculations listed in Appendix A. Sources of mineral–fluid fractionation equation are noted in the text. Meteoric Water and Kaolinite lines and Primary Magmatic Water (PMW) and Felsic Magmatic Water (FMW) boxes are plotted for reference. Dashed line connects South Mountain porphyry biotite (solid diamond) with its equilibrium water (see text). Open diamonds connected by open arrows signify calculated oxygen- and hydrogen-isotope intrusion–water exchange track for a fluid cooling during and following migration to the top of a crystallizing intrusion prior to release to the superjacent vein system. Various mixing and exchange processes capable of modifying fluid or mineral isotopic compositions are indicated by shaded arrows (see text).

Temperatures were taken from alunite–pyrite sulfur-isotope geothermometry where available, and otherwise were estimated from the sample location. Values for alunite and associated fluids are plotted in Fig. 12 along with those for alteration kaolinite as discussed below. The δD_{H2O} values of the fluids causing alunite alteration are substantially different from those of meteoric water at the time of mineralization and require a dominantly magmatic source. The data for alunite from the main zone of alteration–mineralization fall into two groups defined by their δD values, one group with δD values from −70‰ to −61‰ and the other with values from −50‰ to −38‰. All alunite samples from the first group are from elevations below 3600 m, and all but one of the second group are from elevations above 3600 m. It is convenient to label these two groups as *Proximal* and *Distal*, respectively, to distinguish them from each other and from the pyrite–alunite pair from deep in the system. The data in Fig. 12 suggest a trend toward lower $\delta^{18}O$ at increasing δD for the distal (shallow) samples, and toward both lower $\delta^{18}O$ and δD for the proximal (intermediate-depth samples). These patterns suggest several possible physical or chemical processes, as indicated by the shaded arrows in Fig. 12, that shifted the $\delta^{18}O_{H2O}$ of the fluids to values lower than that of the evolved magmatic water, and produced a roughly 40‰ spread in δD.

The isotopic effects due to condensation in the vapor plume or to boiling are not known because of the lack of suitable experimental fractionation factors for saline fluids. These fractionations cannot be large

because the range of fluid-composition values is not exceptional; however, it is likely that boiling and condensation contributed to some of the isotopic variation of the fluid.

We interpret the trend for the distal samples to represent a modification of the isotopic composition of evolved magmatic water in fluids by further exchange with wallrocks at low water–rock ratios during acid-sulfate alteration. Such a shift would be expected to result from the intense leaching that led to the formation of the vuggy-silica ledges and to the replacement of feldspar by alunite.

Mixing of evolved magmatic with unexchanged meteoric water would shift fluid compositions to lower δD_{OH} and $\delta^{18}O_{OH}$ values, and could be the cause of the trend in values for the proximal alunite samples indicated in Fig. 12. Alternatively, in the fracture zone above the brittle–ductile transition, the mixing of fluids that underwent exchange during acid-sulfate alteration (as for the distal alunite) with highly exchanged meteoric waters could also produce such a trend. The maximum amount of incorporation of meteoric water during mixing by either scenario is only 20%.

A more probable explanation for the values of the proximal samples is retrograde exchange of hydrogen with later fluids, most likely those responsible for Cu–Au mineralization. The previously discussed failure of the intramineral SO_4–OH oxygen-isotope geothermometer shows that the two oxygen sites are out of isotopic equilibrium, most likely because of the retrograde exchange of oxygen with later fluids. Kaolinite formed during acid-sulfate alteration can also be interpreted to have undergone retrograde exchange with later fluids. The $\delta^{18}O$ values of fluids responsible for kaolinite formation during acid-sulfate alteration, calculated using the fractionation curves of Sheppard and Gilg (1996) and assuming a temperature of 200 °C, are similar to those obtained for alunite. The δD_{H2O} values, calculated using the equations of Gilg and Sheppard (1996), extend, however, to lower values (Fig. 12). Two interpretations for the greater range of δD values of the kaolinite-forming fluids are that (1) alunite formed from dominantly evolved magmatic water whereas kaolinite formed in dilution zones as evolved magmatic fluids mixed with surrounding exchanged meteoric water, and (2) both alunite and kaolinite formed from dominantly evolved magmatic water, but kaolinite underwent retrograde hydrogen isotopic exchange with highly exchanged meteoric waters as proposed above for the deep alunite samples. The data alone are insufficient to choose between these possibilities, but Kharaka and O'Neil (1976) demonstrated that clays are susceptible to hydrogen- than oxygen-isotope exchange, and that the rate of exchange is a function of temperature and grain size. In addition, as part of this study of the isotopic composition of kaolinite, a 5-m traverse was sampled perpendicular to the Science vein to look for an increase in the meteoric component of the fluids away from the vein, as would be indicated by a decrease in δD and, possibly, $\delta^{18}O$ values (samples SUM-G-W-88[1 through 5], SUM-F-W-88, and SUM-I-W-88[1 and 2]). With the exception of the final sample, which was within 1.5 m of the enclosing smectite zone, the δD values are constant within analytical error. The δD_{H2O} values calculated from the kaolinite data are almost identical to those for alunite in the adjacent quartz–alunite zone (samples SUM-D-W-88 1and 2). This indicates that the δD values in the transition from quartz–alunite, through the kaolinite to the illite alteration zones reflect precipitation from condensed, dominantly magmatic water. At least at this locality, the kaolinite zone was developed by wallrock neutralization with minimal mixing with the surrounding meteoric water.

The alunite of the acid-sulfate alteration zones is much coarser grained than the kaolinite and, therefore, presumably was less susceptible to retrograde exchange with later fluids. We prefer to interpret the trend toward lower values of δD for both the kaolinite and proximal alunite data to indicate retrograde exchange with highly exchanged meteoric waters. In any event, the correspondence of the $\delta^{18}O_{H2O}$ of the alunite and kaolinite parental fluids indicates that both were buffered to the same degree by exchange with wallrocks.

The $\delta^{18}O$ values determined on fine-grained quartz in the groundmass of vuggy-silica, quartz–alunite, and quartz–kaolinite alteration zones are similar at a given locality, and drusy quartz in vugs has the same values as does quartz from the fine-grained groundmass. The values overlap those reported by Larson and Taylor (1987) for similar material from Summitville. The $\delta^{18}O$ values of quartz from the upper (main) portions of the system fall on a broad trend that decreases with depth (Fig. 13a). Inasmuch as quartz–water oxygen-isotope fractionations decrease with temperature, this general

decrease in the $\delta^{18}O$ data of quartz reflects the temperature gradient in the upper part of the deposit as documented by fluid-inclusion homogenization and sulfur-isotope pyrite–alunite fractionation data. The spread of the data into a broad band is due to variations in $\delta^{18}O_{H2O}$ and temperature between samples.

The δD values of alunite also generally decrease with depth (Fig. 13b), but this decrease cannot be due to the temperature gradient that governs the $\delta^{18}O_{quartz}$ data because hydrogen isotopic fractionation factors for alunite–water do not decrease with increasing temperature, as do the fractionation factors for quartz–water. The trend of the δD data most likely reflects increasingly greater degrees of exchange with depth between alunite and waters having an exchanged meteoric water component. As previously mentioned, the shift in the $\delta^{18}O$ of the OH values in alunite due to retrograde exchange with later fluids is considered to be the reason that the $\delta^{18}O_{SO4-OH}$ values do not give valid temperatures and that the deeper alunite sample group has lower δD values than does the shallow group.

5.2.3. Main ore stage and stockwork vein fluids

Isotopic analysis of water in inclusion fluids obtained by crushing a single enargite sample in a vacuum yielded $\delta^{18}O$ and δD values of 0.0‰ and −66‰, respectively (Fig. 14). The δD_{H2O} value is ~30‰ lower than those for the fluids in distal alunite, is slightly lower than those for the alunite proximal fluids, and is approximately 30‰ larger than the values for the fluids for mineralization-stage kaolinite. The $\delta^{18}O_{H2O}$ value from the enargite sample, however, is similar to those for the fluids in kaolinite. The similarities of $\delta^{18}O_{H2O}$ and δD_{H2O} values for the fluids from enargite and from those for the proximal alunite samples suggest that it was with the mineralizing fluids that the proximal alunite underwent retrograde exchange.

In Fig. 14, the δD_{H2O}–$\delta^{18}O_{H2O}$ in enargite inclusion fluids lie along a mixing trend between evolved magmatic fluids and unexchanged or partly exchanged meteoric waters. The high salinities of inclusions in quartz associated with the enargite+pyrite+gold assemblage, supported by studies of secondary inclusions in quartz phenocrysts, indicate that the enargite inclusion fluids were highly saline brines. The magmatic component of the enargite inclusion fluids was likely the dense saline counterpart of the vapor that produced the acid-sulfate alteration. The interpretation of the Summitville enargite-forming fluid as a mixture of evolved magmatic and unexchanged, or partly exchanged, meteoric waters therefore seems reasonable. Detailed studies of main-stage mineralization at Julcani (Deen, 1990; Deen et al., 1994), Lepanto (Hedenquist et al., 1994), and El Salvador (Watanabe and Hedenquist, 2001) indicate that fluids of magmatic origin mixed with unexchanged meteoric water during ore deposition at those

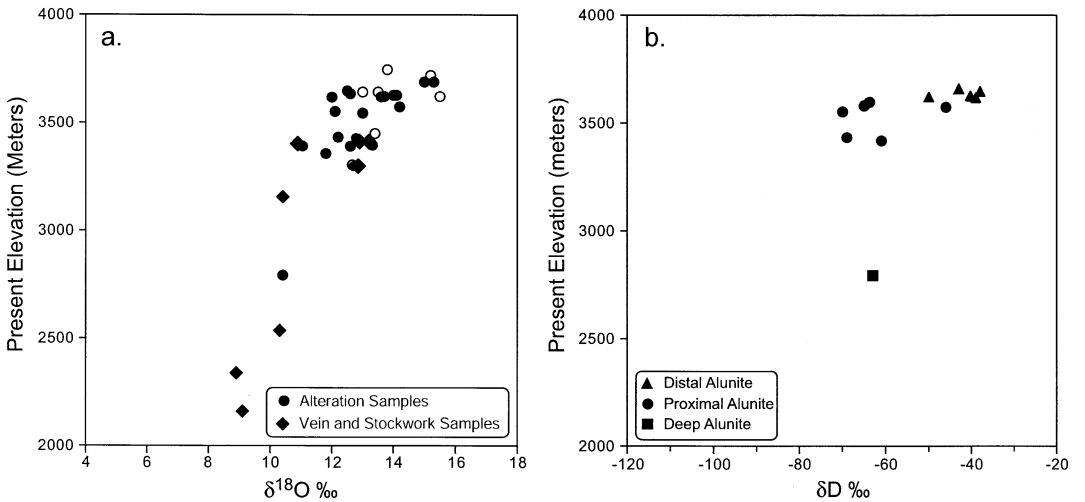

Fig. 13. Variation in $\delta^{18}O$ in quartz and δD in alunite with elevation. (a) $\delta^{18}O$ in alteration and vein and stockwork quartz. Solid symbols, this study; open circles, Larson and Taylor (1987). (b) δD in alunite.

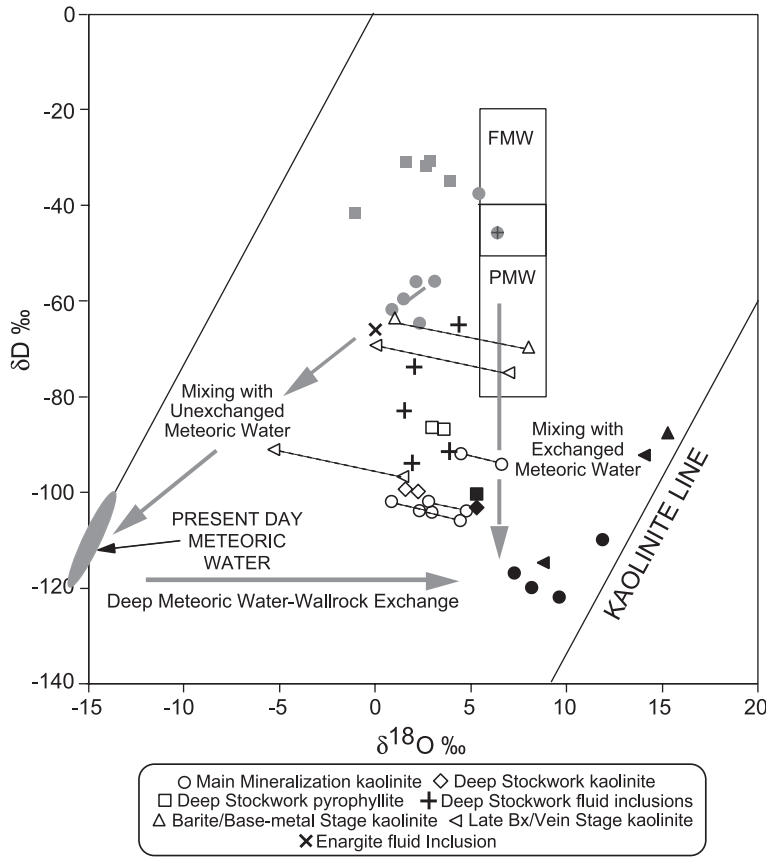

Fig. 14. Plot of $\delta^{18}O$ vs. δD values for vein- or mineralization-related kaolinite and pyrophyllite (solid symbols) and fluids (open symbols) calculated from minerals or measured directly on inclusion fluids. Dashed lines connect fluids calculated at different temperatures from the same mineral value. Temperatures used for fluid calculations are listed in Appendix A. Sources of the mineral–fluid fractionation equation are noted in the text. Alunite data from Fig. 12 are shown as shaded symbols for comparison. Meteoric Water and Kaolinite lines and Primary Magmatic Water (PMW) and Felsic Magmatic Water (FMW) boxes plotted for reference. Shaded arrows indicate mixing or water–rock exchange processes that affect isotopic composition of fluids.

deposits. However, hydrogen and oxygen isotopic data on associated kaolinite and on fluid inclusions in deep stockwork veins, discussed below, suggest that deep mixing with highly exchanged meteoric water may also have played a role in ore-forming fluid history at Summitville. Similar data for kaolinite have been recorded from Lapanto (Hedenquist et al., 1998) and Pierina (Fifarek and Rye, this issue).

The δD_{H2O} values of fluids that formed kaolinite associated with the enargite–covellite–pyrite assemblage, calculated for temperatures of 200 and 250 °C, are substantially lower than those measured from the fluid inclusions in enargite (Fig. 14). The calculated δD_{H2O} and $\delta^{18}O_{H2O}$ values plot at the lower end of a near-vertical band that includes the enargite inclusion fluids and the deeper group of samples of alteration alunite. The trend also includes δD_{H2O}–$\delta^{18}O_{H2O}$ values for the inclusion fluids from stockwork quartz veins sampled from DDH-14, as well as the fluids in equilibrium with kaolinite and pyrophyllite associated with the stockwork veins. Values of $\delta^{18}O_{H2O}$ for the inclusion fluids were calculated from values measured on the quartz host. Values for the kaolinite and pyrophyllite fluids were calculated for temperatures of 300 and 325 °C, and 350 and 400 °C, respectively, recognizing the higher temperature stability of pyrophyllite.

The vertical trend of the δD_{H2O}–$\delta^{18}O_{H2O}$ values of main-stage and stockwork fluids in Fig. 14 suggests

mixing of evolved magmatic fluids with meteoric waters that underwent extensive water–rock exchange at low water–rock ratios deep in the system. There is no evidence to indicate unequivocally at what stage of evolution of the system either the fluids in the inclusions in the stockwork quartz veins were trapped, or the associated kaolinite and pyrophyllite were deposited, but the presence of enargite and covellite in the quartz veins and the presence of high-salinity fluids indicated by the presence of daughter minerals in some fluid inclusions suggest that the stockwork likely formed from main-stage ore fluids, at least in part.

It is possible that the stockwork kaolinite formed at lower temperatures than that assumed for calculation (200–250 °C) and therefore the δD_{H2O} and $\delta^{18}O_{H2O}$ of the fluids indicate mixing with a less-exchanged meteoric water, but such cannot be the case for the pyrophyllite. It is also possible that the kaolinite and pyrophyllite underwent retrograde hydrogen but not oxygen isotopic exchange and that the fluid inclusion δD_{H2O} values, determined by bulk crushing, reflect sampling of mixtures of evolved magmatic and meteoric water. If such is the case, the vertical δD_{H2O} trend of the kaolinite and pyrophyllite data may not be real, and the true δD_{H2O} and $\delta^{18}O_{H2O}$ values may be close to those for the enargite inclusion fluids. Taken at face value, however, the data indicate that mixing of evolved magmatic brines with highly exchanged meteoric waters deep in the system played a role in the development of the main-stage mineralizing fluids at Summitville. Such a mixing scenario is reasonable, if not expectable, and is our preferred interpretation.

5.2.4. Fluids of the barite–base-metal stage

Sparse, narrow barite veins cut breccias (hydrothermal breccias of Gray and Coolbaugh, 1994) that cut the main-stage mineralization. In the deeper parts of the open pit, these barite veins also contain galena, sphalerite, and pyrite. At shallower levels, base metals are absent and goethite and jarosite occur with the barite. Barite veins from both environments contain gold, but the shallow veins are typically much richer. Gray and Coolbaugh (1994) suggested that the oxidized-Fe minerals associated with barite in the shallow part of the system resulted from supergene oxidation. Stoffregen (1987), noting the fluid-inclusion homogenization temperature estimates of Cunningham (1985), suggested that the jarosite and goethite, along with the barite, base metals, and gold, were not weathering products but instead formed by the mixing of hypogene fluids and steam-heated waters that had drained back into the ore zone, a process discussed by Reed and Spycher (1986). Ebert and Rye (1997) proposed a similar process for the secondary enrichment of gold in the low-sulfidation Crofoot-Lewis gold deposit in the Sulphur district, Nevada. Barite deposition typically occurs during mixing of fluids (Holland and Malinin, 1979).

The $\delta^{18}O_{SO4}$ values for most barite samples are slightly lower than the values for alteration alunite at corresponding $\delta^{34}S$ values (Fig. 15). In large part, this results from the difference between alunite–water and barite–water oxygen-isotope fractionations but may also be due, in part, to a greater influence of meteoric water on the $\delta^{18}O_{SO4}$ of the barite, and to temperature variations. The aqueous sulfate for most of the barite equilibrated with fluids that had almost the same $\delta^{34}S_{SO4}$ and $\delta^{18}O_{H2O}$ as did the alunite alteration and was clearly derived from magmatic sources. Consistent with a magmatic fluid source for the aqueous sulfate, a sample of kaolinite (JG-1918) associated with barite and sphalerite has $\delta^{18}O$ and δD values of 15.4‰ and

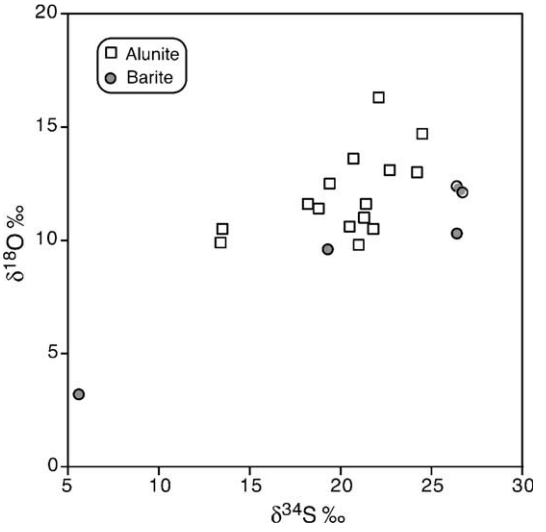

Fig. 15. Plot of $\delta^{18}O$ vs. $\delta^{34}S$ for barite and alunite samples. The correspondence of $\delta^{34}S$ and $\delta^{18}O$ values with those for alunite for all but one barite sample indicates that the sulfate in those barite samples was of magmatic origin. The much lower values of 5.8‰ and 3.2‰ for the single barite suggests that its sulfate had approached equilibrium with steam-heated waters whose sulfate was derived from the oxidation of H_2S. See text for discussion.

−88‰, respectively. The $\delta^{18}O_{H2O}$ and δD_{H2O} values of associated fluids at temperatures of 100 to 150 °C are 1.0‰ to 5.2‰, and −64‰ to −68‰, respectively (Fig. 14), indicating a large component of magmatic water. Not all aqueous sulfate in the barite was magmatic. A sample of barite (PMB SV-2-85) with a $\delta^{34}S$ value of only 5.6 ‰ and a low $\delta^{18}O_{SO4}$ value of 3.2 ‰ (Fig. 15) was collected at an elevation of ~3650 m and is associated with goethite and significant Au values. If the temperature of barite deposition was ≤150 °C, the $\delta^{18}O_{H2O}$ of the parent fluid was ≤−8‰, indicating a substantial meteoric component. The major component of aqueous sulfate for this sample was most likely derived from the oxidation of H_2S in a steam-heated environment overlying the main alteration–mineralization zone. In the more neutral and lower temperature of solutions typical of barite deposition during late-stage fluid mixing, sulfur-isotope exchange between aqueous sulfate and sulfide is kinetically inhibited (Ohmoto and Lasaga, 1982); thus, isotopic disequilibrium among sulfur species would be reflected in the precipitated barite. Getahun (1994) reported the presence of a rubbly, chalcedony-rich zone containing fine-grained alunite directly above the top of the open pit. He interpreted this material to represent a steam-heated zone. No alunite samples have been analyzed from this zone.

We propose that fluids that deposited most veins of barite+base metals at Summitville, like those for the main Cu–Au mineralization, were dominated by the aqueous sulfate derived from residual brines near the brittle–ductile transition, and that the fluids represent a further neutralization of the system. Variable degrees of mixing of such fluids with overlying steam-heated waters during the late-stage collapse of the hydrothermal system are likely to have occurred, as at Pierina, Peru (Fifarek and Rye, this issue). However, except for the single barite whose $\delta^{18}O_{SO4}$ indicated a substantial meteoric component, mixing of magmatic and steam-heated waters leading to barite deposition has not been well documented at Summitville.

5.2.5. Fluids related to late veins of fine-grained alunite

Narrow, fine-grained monomineralic alunite veins occur at scattered locations at Summitville. Stoffregen (1987) considered them to be related to the veins of barite+base metals, and Gray and Coolbaugh (1994) thought the veins to be supergene. Two such samples have been analyzed (Appendix A). The $\delta^{34}S$ and $\delta^{18}O_{SO4}$ values of 13.4‰ and 9.9‰, respectively, of sample 328-108 are nearly identical to those for deep alunite sample DDH-14-2667. If these are equilibrium values, they imply that either the alunite was formed at unreasonably high temperatures for such an elevation or from fluids with abnormally low $\delta^{34}S$ values for aqueous sulfate. Because sample 328-108 is paragenetically late, its sulfur isotopic value may reflect some oxidation of isotopically light sulfide, possibly related to an influx of oxygenated groundwater in the upper part of the deposit. However, it seems more likely that the alunite has a magmatic-steam origin related to decompression deep in the hydrothermal system. The low $\delta^{34}S$ and the large $\delta^{18}O_{SO4–OH}$ values are consistent with such an origin, as is the vein occurrence and lack of associated pyrite (Rye et al., 1992). Sample SUM-1-88 is a fine-grained vein selvage of pure alunite. Except for a large $\delta^{34}S$ value (24.5‰), SUM-1-88a also has isotopic characteristics of magmatic-steam alunite (δD=−46‰), and we interpret the alunite also to have formed in that environment. Minor veins of magmatic-steam alunite are known to have formed during the final stages of the system that produced the large magmatic-hydrothermal alunite deposit at Red Mountain, Lake City, Colorado (Bove et al., 1990; Rye, 1993).

5.2.6. Fluids related to late kaolinite-matrix breccias

Breccias with kaolinite matrices that carried high Au values represent the latest hydrothermal event at Summitville. Four samples yielded ranges of $\delta^{18}O$ and δD of 9.0‰ to 15‰, and −115‰ to −89‰, respectively (Appendix A). There is no evidence to constrain the temperatures of deposition of the samples, but their lateness in the paragenesis suggests formation at lower temperatures than those for earlier kaolinite. Accordingly, $\delta^{18}O_{H2O}$–δD_{H2O} values of parent fluids were calculated for 100 and 150 °C. If calculated for 100 °C, the $\delta^{18}O_{H2O}$–δD_{H2O} values of fluids for sample 257-214 are very close to those for the enargite fluid inclusions, and similarly calculated values for sample 317-1156 plot close to the magmatic water–meteoric water mixing line. The value of $\delta^{18}O_{H_2O}$ for sample 257-214 at 150 °C is −5.2 larger than that for any other calculated fluid (Fig. 14) and suggesting that the sample formed closer

to the assumed 100 °C temperature. Given the lack of independent temperature data, no definite conclusions can be drawn about the origin of the fluids.

5.3. $\delta^{34}S_{\Sigma S}$ and redox state of system

The $\delta^{34}S$ of the bulk sulfur in the magma and in the fluids that exsolved from it can be estimated from $\delta^{34}S$ data on igneous minerals if data on the temperature, sulfur fugacity, and oxidation state of the magma are available. Currently, such data do not exist for the South Mountain quartz latite. However, such an estimate can be made from the $\delta^{34}S$ data on sulfate in apatite and chalcopyrite inclusions in biotite and magnetite. As discussed in Section 5.1.1, the $\delta^{34}S$ values of chalcopyrite in both biotite and magnetite appear to represent postcrystallization retrograde exchange with magmatic sulfur. An adjusted value of $\delta^{34}S$ of chalcopyrite in equilibrium with sulfate in apatite at 780 °C of −0.3‰ was calculated using the fractionation factors of Ohmoto and Lasaga (1982). If this value is a reasonable estimate, the $\delta^{34}S$ of the bulk sulfur in the magma lies between it and the $\delta^{34}S$ of the apatite (5.5‰), the exact value depending on the proportions of reduced and oxidized sulfur species in the magma, and, therefore, its redox state.

Estimates of both $\delta^{34}S$ of the magma and SO_4^{2-}/H_2S_{aq} of fluids separated from it can be obtained from a plot of $\delta^{34}S$ of H_2S_{aq} in equilibrium with sulfide minerals vs. $\delta^{34}S$ of SO_4^{2-} in equilibrium with coexisting sulfate minerals, assuming that equilibrium obtained between the aqueous species in the fluids.

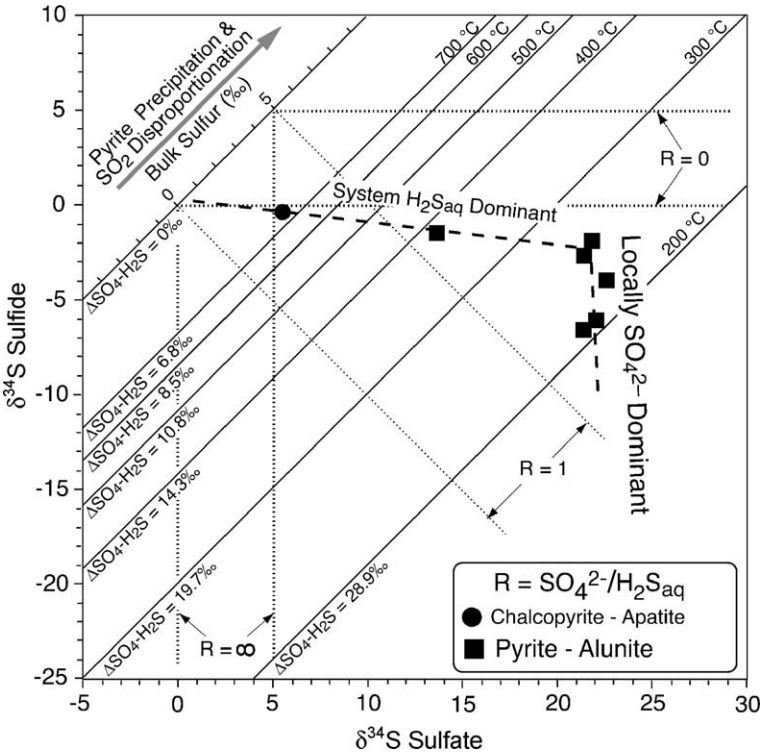

Fig. 16. Diagram of δ–δ for $\delta^{34}S$ in aqueous sulfide and sulfate species in equilibrium with chalcopyrite in biotite and magnetite phenocrysts and apatite (circle), and pyrite and alunite pairs (squares) formed during acid-sulfate alteration. The nearly horizontal slope of the dashed line through the chalcopyrite–apatite point, the deep pyrite–alunite point, and the 250 °C pyrite–alunite points indicates that the system was H_2S_{aq}-dominant in the magma and during ascent into the acid-sulfate alteration zone due to buffering by the wallrocks. Extrapolation of the dashed line to the 45° line for $\Delta^{34}SO_4$–H_2S=0‰ shows that the initial isotopic composition of the bulk sulfur in the system was near 0‰ and remained so until reaching the zone of intense acid-sulfate alteration. Precipitation of pyrite and increasing disproportionation of SO_2 during wallrock alteration changed the bulk isotopic composition of the aqueous sulfur species to increasingly larger values, as indicated by the shaded arrow, causing the fluids to become SO_4^{2-}-dominant.

Fig. 16 is such a plot for alunite–pyrite pairs produced by acid-sulfate alteration along with the adjusted value for igneous apatite and chalcopyrite inclusions in magnetite and biotite. The theoretical and mathematical basis for δ–δ diagrams was developed for oxygen-isotope data by Gregory and Criss (1986) and Criss et al. (1987). It has been adapted for sulfur isotopes by Fifarek and Rye (this issue) and Rye (this issue). In Fig. 16, values of H_2S_{aq} in equilibrium with the sulfide minerals, calculated from the equations of Ohmoto and Rye (1979), are plotted against the $\delta^{34}S$ of the sulfate mineral on the assumption that the sulfur-isotope fractionation between sulfate minerals and SO_4^{2-} is negligible over the temperature range considered. Lines of constant ΔSO_4^{2-}–H_2S_{aq} with a positive 1:1 slope are plotted for temperatures from 200 to 700 °C on the basis of the equations of Ohmoto and Lasaga (1982). A line representing ΔSO_4–H_2S=0‰ is also plotted and scaled for $\delta^{34}S$ for the bulk sulfur in the system. Dotted lines representing R values (R=SO_4^{2-}/H_2S_{aq}) of 0, 1, and infinity are plotted for bulk sulfur $\delta^{34}S$ values of 0‰ and 5‰. Note that, due to the lack of consistency between fractionation equations, the data points plot close to, but not on, the ΔSO_4–H_2S lines for their temperatures estimated from the pyrite–alunite fractionation. Although Fig. 16 cannot be used in a strict analytical sense, the geometry of the plot allows estimates of the evolution of the bulk sulfur and the SO_4^{2-}/H_2S_{aq} of the system. The dashed line through the points for two 250 and 380 °C pyrite–alunite pairs and the apatite–chalcopyrite$_{adjusted}$ pair indicates that the fluid was H_2S_{aq}-dominant at an almost constant SO_4^{2-}/H_2S of roughly 0.18 during its ascent from the carapace of the source magma, implying that the system was buffered by the wallrocks during ascent. During the intense leaching leading to the vuggy-silica alteration, the combined processes of SO_2 disproportionation and pyrite deposition changed the bulk ^{34}S of the system and the fluid became strongly SO_4^{2-}-dominant as indicated by the nearly vertical dashed line through the pyrite–alunite points, the wallrocks having lost their buffering capacity. This evolution of the redox state of the sulfur species from dominantly reduced to dominantly oxidized is obvious from the fact that, in the quartz–alunite alteration zone, the $\delta^{34}S$ of the sulfate is nearly constant while that for the pyrite undergoes a much greater change.

As noted in Section 5.2.4, the $\delta^{34}S$ values for barite samples are similar to those for pre-ore alunite, except for the one sample interpreted to have been precipitated from fluids involving steam-heated waters. The large $\delta^{34}S$ values for these barite samples, and the $\Delta^{34}S$ between barite and associated sulfides, are similar enough to those for the pre-ore alunite and pyrite to indicate that the late-stage ore fluids had a sulfur isotopic geochemistry similar to that of the earlier acid-sulfate fluids. This reflects the conclusion that the oxidation state of the fluids for both stages was buffered by the same deep rocks that controlled the H_2S/SO_4^{2-} of the alunite alteration fluids at a value >1 prior to disproportionation of SO_2.

6. Summary of the evolution of the hydrothermal system

6.1. Models of epithermal high-sulfidation systems

It is useful to consider the Summitville deposit in terms of recent models for the formation of epithermal high-sulfidation ore deposits. Such models are built on concepts of Sillitoe (1973, 1983, 1995), Henley and McNabb (1978), Burnham (1979), White (1991), Rye et al. (1992), Giggenbach (1992, 1997), Fournier (1987, 1999), Rye (1993), Hedenquist and Lowenstern (1994), Hedenquist et al. (1994, 1998) and others. Arribas (1995) comprehensively discussed the models presented by various authors. More recent models include those by Hedenquist et al. (1998), Muntean and Einaudi (2001), Rye (this issue), Fifarek and Rye (this issue), and Deyell et al. (this issue).

Almost all models consider epithermal high-sulfidation deposits to have formed in magmatic-hydrothermal systems driven by epizonal magmatic intrusions. Most relate the epithermal deposits to deeper porphyry-style mineralization as proposed by Sillitoe (1973) although many deposits show no evidence of such a relationship (cf. Sillitoe, 1989). In most models, an early stage of acid-sulfate alteration is attributed to the condensation of a magmatic vapor plume, and subsequent Cu–Au–Ag mineralization to precipitation from a condensed fluid, often with a significant meteoric water component. Some models, however, attribute both alteration and mineralization to be products of the vapor plume. Other differences

among models include the depth, mechanisms and timing of generation of the vapor plume and later mineralizing fluid, and the cooling paths and degree of fluid interaction with magma and wallrocks.

Most models are synoptic, but of those, many have been developed in reference to specific deposits or occurrence types. It is therefore likely that many of the differences among the models reflect differences in size and depth of intrusion, volcano–tectonic environment, hydrologic regime, and the timing of fluid evolution. In addition, differences related to multiple magmatic events with possible different degrees of magma/fluid–crustal interaction may lead to differences in the isotopic, mineralogical, and geochemical signatures between deposits.

6.2. Evolution of the Summitville hydrothermal system

The alteration and mineralization at Summitville were integral parts of the magmatic system responsible for the emplacement of the quartz latite volcanic dome of South Mountain. The fluids responsible for the alteration and mineralization are presumed to have been derived from a magma that produced the quartz monzonite stock emplaced in the roots of the nearly coeval volcanic dome. Multiple episodes of brecciation before, during, and following mineralization and alteration attest to the dynamic nature of the system.

The shallow portion of the hydrothermal system evolved in time from an initially low-pH, high-sulfidation system to a more nearly neutral, low-sulfidation system. The initial hydrothermal event was the intense acid-sulfate alteration of the South Mountain volcanic dome. The sulfuric acid principally responsible for the intense alteration was produced by the disproportionation of SO_2 during condensation of a magmatic vapor plume. Subsequently, Cu–Au mineralization was deposited from a high-salinity brine. Crystallization of anhydrous minerals in the cooling magma chamber resulted in exsolution of a moderate-salinity brine, probably beginning somewhere near 780 °C. As the intrusion crystallized, the fluids rose and accumulated in and below the crystalline, but still plastic, carapace of the magma chamber under lithostatic pressure just below the brittle–ductile transition at a depth of ~1.5 km and a temperature ~400 °C. Isotopic exchange with the rocks of the carapace and subjacent magma during cooling and migration caused the $\delta^{18}O_{H2O}$ and δD_{H2O} of the fluid to evolve from initial values of approximately 8‰ and −70‰ at 780 °C to 2‰ and −45‰ at 400 °C. Thus, the magmatic fluid from which the vapor plume and corresponding high-salinity brine were generated was an *evolved* fluid, whose δH_{H2O} and $\delta^{18}O_{H2O}$ differed substantially from those of the initial magmatic fluid. Reaction with the carapace rocks also buffered the redox state of the fluids at a level in which H_2S dominated the sulfurous species in the deeper part of the system.

Release of the evolved magmatic fluids into the superjacent hydrostatically pressured brittle-fracture zone, due to downward migration of the brittle–ductile transition, tectonically induced increase in strain rate, or hydrofracting, resulted in the separation of the moderate-salinity brine into both a low-density (vapor) phase of very low salinity and a hypersaline brine. Volatiles, such as H_2S, SO_2, and HCl, were preferentially partitioned into the low-density phase. Because of its low density, the vapor plume rose along fractures, whereas the higher density hypersaline brine remained deep in the system. Disproportionation of SO_2 into H_2S and H_2SO_4 as the vapor plume condensed on cooling, together with dissociation of HCl, produced highly reactive low-pH fluids. The origin of the vapor plume by separation from evolved magmatic fluid is documented by the δD and $\delta^{18}O$ values of the replacement alunite. There is little evidence that the plume condensed into or mixed with significant (>20%) amounts of meteoric water. Some replacement alunite underwent retrograde exchange with later fluids that contained a significant component of probably exchanged meteoric water.

As the fluids attacked the wallrocks in the acid-sulfate alteration zone, their $\delta^{18}O_{H2O}$ values decreased and, depending on water–rock ratios, δD_{H2O} values increased. Concurrently, precipitation of pyrite and continued disproportionation of SO_2 increasingly controlled the sulfur chemistry of the fluids. Eventual SO_4^{2-} dominance in the fluids is evident in that the main variation in $\delta^{34}S$ values of coexisting alunite and pyrite occurs in the pyrite rather than alunite at higher elevations. Increasing neutralization of the fluids away from the veins by reaction with wallrocks led to the alteration zoning from vuggy-silica through quartz–alunite and quartz–kaolinite/illite to smectite zones.

Whereas the vapor plume rose along fractures because of its low density, the hypersaline brine remained deep in the fracture zone just above the brittle–ductile transition. Possibly as a result of mixing with surrounding meteoric waters and consequent dilution, perhaps coupled with pressure release on the fluids, the brines rose by advection, carrying the ore components with them as a result of their high ligand content. These ore fluids likely formed the pyrite–quartz stockwork veins deep in the system. Mixing of the brines with meteoric water, either in the ore zone or deep in the system, or both, is indicated by the $\delta^{18}O$–δD values of kaolinite that accompanies the ore and the alteration zone in the stockwork, and by the δD_{H2O} values of inclusion fluids in the stockwork quartz.

Most late veins of barite–base metals seem to have been deposited from fluids isotopically similar to those that deposited the Cu–Au–Ag ores. The barite-bearing veins likely represent further mixing of the brine with meteoric water and mark the final evolution of the system from a low-pH high-sulfidation system to a near-neutral low-sulfidation system. Kaolinite in kaolinite-matrix breccias, formed during the latest hydrothermal event, has $\delta^{18}O$ and δD values similar to those of the ore-stage kaolinite and was deposited from similar fluids. The breccias contain gold but are devoid of sulfide minerals. The relationship of these breccias to the main ore stage and the barite–base-metal mineralization is unknown. The possible role of a descending steam-heated system in the formation of the late-stage veins of barite–base metals at Summitville cannot be evaluated on present data, but study of additional samples might provide needed insight.

The proposed evolution of the Summitville hydrothermal system is consistent with the major aspects of most models. These include the close relationship in time and space to silicic epizonal intrusions, the generation of intense acid-sulfate alteration by reaction of wallrocks with sulfuric acid generated by the disproportionation of SO_2 during condensation of a vapor plume, and the time progression from alteration to high-sulfidation enargite+covellite+gold mineralization to low-sulfidation base-metal+barite mineralization. The evolution, however, differs from most models in the proposed prerelease isotopic exchange of the primary magmatic waters with the cooling intrusion, and with some models in the proposed cogeneration of the vapor plume and the later mineralizing brines, as well as the depth of release and P–T evolution of the brines during ascent. The degree of shallow mixing of the magmatic fluids with surrounding meteoric waters at Summitville is less than that for other deposits, such as Julcani (Deen et al., 1994) and Lepanto (Hedenquist et al., 1998), but the data indicate a high degree of mixing deep in the system, not described in other models.

The above discussion describes the evolution of the Summitville system as a simple, linear progression. In reality, evolution was much more complex in spite of the system's relative simplicity. For example, brecciation which was contemporaneous with acid-sulfate alteration, brecciation between main-stage mineralization and barite–base-metal mineralization, and brecciation following barite–base-metal mineralization suggest that hydrothermal activity was probably periodically punctuated by bursts of magmatic steam. The presence of sparse veins of fine-grained alunite with isotopic characteristics of magmatic-steam alunite further attests to the dynamic nature of the system. In addition, although evidence is scant, it is likely that a steam-heated system developed at shallow levels during the late stages of the system.

Acknowledgements

Mike Wasserman made many of the isotopic analyses. Carol Gent made additional analyses. The assistance of Mark Coolbaugh and M. Stephen Enders, then of the Galactic Mining Company, is very much appreciated. Not only did they share their knowledge of the Summitville deposit, and were they generous with their time and guidance during field visits, they made available a large amount of exploration diamond-drill core to the USGS Core Research Center in Denver, where it is stored and available for further study. John Gray of the USGS provided additional samples for study. Greg Symmes made the fluid-inclusion thermometric measurements on sample 293-37. Discussions with Skip Cunningham, Paul Barton, Gary Landis, and Tom Steven helped shape our concepts. Reviews by C.G. (Skip) Cunningham, Rich Fifarek, and Robert Seal significantly improved the manuscript. **[PD]**

Appendix A. Data for stable isotopes, Summitville, Colorado

Sample number[a]	Alteration zone	Location	Elevation (m)	Northing	Easting	Mineral	$\delta^{34}S$	$\delta^{18}O_{SO_4}$	$\delta^{18}O_{OH}$	δD	$\delta^{18}O$	$\delta^{18}O_{H_2O}$	δD_{H_2O}[b]	T[c] (°C)
Magmatic stage														
235-1349a		South Mountain	3249.8	50,653	99,994	Whole rock					7.3			
235-1349b		South Mountain	3249.8	50,653	99,994	Whole rock					7.8			
						K-spar					7.4			
South Mtn Rye		South Mountain	*4000.0*			Biotite				−90	6.7	9.4	−68	780
						Quartz					9.4	9.4		780
						K-spar					8.5	9.3		765
						Apatite	5.5							
						$Chalcopyrite_{(mag)}$	−6.3/−.33							485/780[d]
						$Chalcopyrite_{(bio)}$	−2.3/−.33							670/780[d]
Alteration stage														
Vuggy–silica samples														
320-1026	Vuggy silica	Tewksbury	3356.7	50,655	100,129	Quartz					11.8			
300-713.5	Vuggy silica	Copper-Hill	3402.4	51,144	100,285	Quartz					11.0			
DDH-5-1058	Vuggy silica	Annie	3298.5	52,450	100,345	Quartz					12.7			
300-672.5a	Vuggy silica	Copper-Hill	3412.3	51,176	100,304	Quartz					13.2			
300-672.5b	Vuggy silica	Copper-Hill	3412.3	51,176	100,304	Quartz					12.9			
SUMCW88(1)	Vuggy silica	Science Outcrop	3621.0	*50,475*	*100,625*	Pyrite	−1.2							
321-887	Vuggy silica	Tewksbury	3412.5	50,405	100,093	Pyrite	−8.9							
332-44	Vuggy silica	Hidden	3634.0	50,886	100,306	Quartz					12.6			
331-243.5	Vuggy silica	Tewksbury	3619.6	50,602	100,120	Quartz					13.6			
328-311	Vuggy silica	Annie	3544.2	51,721	99,855	Quartz					13.0			
						Pyrite	−2.7							
323-742	Vuggy silica	French	3390.3	52,209	99,615	Quartz					12.6			
AZTK A	Vuggy silica	McDonald	3627.1	*50,500*	*100,300*	Quartz					14.1			
						Pyrite	−4.5							
AZTK B(ph)	Vugy silica	McDonald	3627.1	*50,500*	*100,300*	Quartz					9.8			
AZTK C	Vugy silica	McDonald	3627.1	*50,500*	*100,300*	Quartz					14.0			
Deep quartz–alunite samples														
DDH-14-2667	Quartz–alunite	Iowa	2792.9	50,502	100,876	Alunite	13.5	10.5	12.3	−63		6.4	−45	390
						Pyrite	−2.2							
						Quartz					10.4			

(continued on next page)

Appendix A (*continued*)

Sample number[a]	Alteration zone	Location	Elevation (m)	Northing	Easting	Mineral	$\delta^{34}S$	$\delta^{18}O_{SO_4}$	$\delta^{18}O_{OH}$	δD	$\delta^{18}O$	$\delta^{18}O_{H_2O}$	δD_{H_2O}[b]	T[c] (°C)
Proximal quartz–alunite samples														
255-629	Quartz–alunite	Annie	3417.5	52,287	99,503	Alunite	21.8	10.5		−61		2.1	−55	250
			3417.5	52,287	99,503	Pyrite	−3.0							
			3417.5	52,287	99,503	Quartz					12.9			
266-716	Quartz–alunite	Copper-Hill	3432.8	50,771	100,321	Alunite	21.4	11.6		−69		0.7	−61	200
			3432.8	50,771	100,321	Pyrite	−8.1							
			3432.8	50,771	100,321	Quartz					12.2			
281-401	Quartz–alunite	Del Norte	3552.1	51,222	99,865	Alunite	21.3	11.0	11.3	−70		2.6	−64	250
			3552.1	51,222	99,865	Pyrite	−3.6							
			3552.1	51,222	99,865	Quartz					12.1			
289-406	Quartz–alunite	West End	3572.8	51,079	98,602	Alunite	22.1	16.3	13.9	−46		5.4	−37	200
			3572.8	51,079	98,602	Pyrite	−7.6							
			3572.8	51,079	98,602	Quartz					14.2			
328-108	Quartz–alunite	Annie	3584.0	51,785	100,009	Alunite	13.4	9.9	7.6	−65		−1.0	−59	*250*
SUM-84-2	Quartz–alunite	Annie	3596.6	*51,850*	*101,050*	Alunite	18.8	11.4		−64		3.0	−55	*250*
Distal quartz–alunite samples														
Sum-12-71	Quartz–alunite	Science Dump	3582.9	*50,475*	*100,625*	Alunite	20.5	10.6						
Sum-11-71	Quartz–alunite	Science Dump	3582.9	*50,475*	*100,625*	Alunite	24.2	13.0						
293-175	Quartz–alunite	N. Tewksbury	3610.0	50,782	100,194	Alunite	19.4	12.5						
332-126	Quartz–alunite	N. Tewksbury	3618.0	50,860	100,244	Alunite	22.7	13.1	12.3	−39		2.8	−30	210
			3618.0	50,860	100,244	Pyrite	−5.4							
			3618.0	50,860	100,244	Quartz					12.0			
SUMDW88(4)	Quartz–alunite	Science Outcrop	3621.0	*50,475*	*100,625*	Alunite	21.0	9.8	9.8	−50		−1.1	−41	*200*
SUMDW88(6)	Quartz–alunite	Science Outcrop	3621.0	*50,475*	*100,625*	Alunite		12.5	12.5	−40		1.6	−31	*200*
293-40	Quartz–alunite	N. Tewksbury	3646.9	50,796	100,253	Alunite	20.7	13.6		−38		2.7	−31	*200*
			3646.9	50,796	100,253	Quartz					12.5			
333-050	Quartz–alunite	Del Norte	3650.1	51,311	99,932	Alunite	18.2	11.6						
333-014	Quartz–alunite	Del Norte	3659.0	51,320	99,953	Alunite	24.5	14.7	16.0	−43		3.8	−34	*200*
Proximal quartz–kaolinite samples														
266-143	Quartz–kaolinite	Copper-Hill	3575.9	51,061	100,586	Kaolinite				−98	12.3	5.0	−80	*250*
257-163	Quartz–kaolinite	Annie	3601.8	51,886	99,703	Kaolinite				−81			−63	*250*
333-227	Quartz–kaolinite	Del Norte	3606.5	51,265	99,830	Kaolinite				−107			−89	*250*
			3606.5	51,265	99,830	Pyrite		−3.0						
Distal quartz–kaolinite samples														
SUM-GW-88-1	Quartz–kaolinite	Science Outcrop	3621.0	*50,475*	*100,625*	Kaolinite				−62			−44	*200*
SUM-GW-88-2	Quartz–kaolinite	Science Outcrop	3621.0	*50,475*	*100,625*	Kaolinite				−61			−43	*200*
SUM-D-W88-3	Quartz–kaolinite	Science Outcrop	3621.0	*50,475*	*100,625*	Kaolinite				−60			−42	*200*
SUM-DW-88-5	Quartz–kaolinite	Science Outcrop	3621.0	*50,475*	*100,625*	Kaolinite				−62	11.5	4.2	−44	*200*

SUM-F-W88	Quartz–Kaolinite	Science Outcrop	3621.0	*50,475*	*100,625*	Kaolinite		−62			−44	*200*
SUM-I-W88-1	Quartz–kaolinite	Science Outcrop	3621.0	*50,475*	*100,625*	Kaolinite		−64			−46	*200*
SUM-I-W88-2	Quartz–kaolinite	Science Outcrop	3621.0	*50,475*	*100,625*	Kaolinite		−83	11.6	4.3	−65	*200*
		Science Outcrop	3621.0	*50,475*	*100,625*	Quartz			13.7			
293-118	Quartz–kaolinite	N. Tewksbury	3625.6	50,788	100,219	Kaolinite		−83			−83	*200*
AZTK 2	Quartz–kaolinite	McDonald	3627.1	*50,500*	*100,300*	Kaolinite		−73				
AZTK 6	Quartz–kaolinite	McDonald	3627.1	*50,500*	*100,300*	Kaolinite		−78			−60	*200*
AZTK 7	Quartz–kaolinite	McDonald	3627.1	*50,500*	*100,300*	Kaolinite		−68			−50	*200*
123(A)	Quartz–kaolinite	Tewksbury	3688.1	*49,500*	*100,800*	Kaolinite		−81	9.0	1.7	−63	*200*
123(B)	Quartz–kaolinite	Tewksbury	3688.1	*49,500*	*100,800*	Kaolinite		−81	9.6	2.3	−63	*200*
			3688.1	*49,500*	*100,800*	Quartz			15.0			
			3688.1	*49,500*	*100,800*	Quartz			15.3			
Main mineralization stage												
DDH-5-1058		Annie	3298.5	52,450	100,345	Kaolinite		−117	7.3	−7.0/0.0	−93/−99	*275–350*
			3298.5	52,450	100,345	Quartz			12.7			
323-899		Annie	3347.6	52,165	99,547	Covellite	−6.7					
320-1026		Tewksbury	3357.3	50,656	100,130	Chalcopyrite	−5.7					
323-744		Annie	3390.3	52,209	99,615	Kaolinite		−120	8.2	−6.1/.09	−96/−102	*200/250*
300-713.5		Copper-Hill	3402.4	51,144	100,285	Chalcopyrite	−18.0					
			3402.4	51,144	100,285	Kaolinite		−122	9.7	−4.6/1.8	−98/−106	*200/250*
			3402.4	51,144	100,285	Quartz			11.0			
300-713		Copper-Hill	3402.5	51,144	100,285	Kaolinite		−107			−83/−89	*200/250*
300-672.5a		Copper-Hill	3412.3	51,176	100,304	Kaolinite			10.8	−4.0/3.0		*200/250*
300-672.5b		Copper-Hill	3412.3	51,176	100,304	Kaolinite			9.3	−5/2.0		*200/250*
			3412.3	51,176	100,304	Quartz			13.2			
			3412.3	51,176	100,304	Quartz			12.9			
255-654.5		Annie	3417.5	52,278	99,503	Covellite	−4.6					
SUM-5-71		Annie (Reynolds Tunnel)	3450.0			Covellite	−3.4					
SUM-4-71		Annie (Reynolds Tunnel)	3450.0			Kaolinite		−110	11.9	−2.4/4.6	−87/−93	*200/250*
			3451.0			Covellite	−6.7					
SUM-88-2		Annie	3566.2	*52,100*	*99,700*	Enargite (Fl. Incl.)				**0.0**	**−66**	
SUM-1-71		Science Dump	3582.9	*50,475*	*100,625*	Enargite	−2.7					
SUM-7-71		Science Dump	3582.9	*50,475*	*100,625*	Galena	−6.6					
SUM-2b-71		Science Dump	3582.9	*50,475*	*100,625*	Pyrite	−3.0					
SUM-2a-71		Science Dump	3582.9	*50,475*	*100,625*	Sulfur	−5.3					
257-204		Annie	3601.8	51,886	99,703	Galena	−1.9					
Deep stockwork veins												
DDH-14-4734	Stockwork	Iowa	2160.0	50,502	100,876	Quartz			9.1	3.8	**−92**	*350*
DDH-14-4161a	Stockwork	Iowa	2337.5	50,502	100,876	Quartz			8.9	2.0	**−94**	*300*
DDH-14-4161b	Stockwork	Iowa	2337.5	50,502	100,876	Quartz			8.0	2.0	**−72**	*350*
DDH-14-4148.5	Stockwork	Iowa	2341.3	50,502	100,876	Pyrophyllite		−100	5.3	3.5/2.8	−87/−88	*350–400*
DDH-14-3498	Stockwork	Iowa	2536.0	50,502	100,876	Quartz			10.3	4.3	**−65**	*325*

(continued on next page)

Appendix A (*continued*)

Sample number[a]	Alteration zone	Location	Elevation (m)	Northing	Easting	Mineral	$\delta^{34}S$	$\delta^{18}O_{SO_4}$	$\delta^{18}O_{OH}$	δD	$\delta^{18}O$	$\delta^{18}O_{H_2O}$	δD_{H_2O}[b]	T[c] (°C)
DDH-14-2056	Stockwork	Iowa	2979.1	50,502	100,876	Kaolinite				−103	5.3	1.6/2.2	−89/−90	300–325
DDH-14-1476	Stockwork	Iowa	3155.9	50,502	100,876	Quartz					10.4	1.5	**−83**	*250*
Barite–base-metal stage														
255-654.5		Annie	3410.8	52,279	99,490	Galena	−7.0							
Hidden vein		Hidden	3596.6	50,900	100,500	Barite	26.5				12.3	1		
ROR-SV- 2-89		Annie	3618.0			Sphalerite	−4.2							*100–200*
			3619.0			Barite	22.6							
Annie		Annie	3627.1	52,100	99,900	Barite	26.6	12.2						
PMB SV-2-85		Copper-Hill	3640.0	50,960	100,646	Barite	5.6				3.2			
JG-1819		Annie	3645.4			Kaolinite				−88	15.4	1.1/8.1	−64/−70	*100–200*
293-38		Tewksbury	3646.9	50,796	100,253	Barite	24.3							
Upper tewksbury		Tewksbury	3657.6	49,500	100,800	Barite	19.3	9.6						
Aztec glory hole		Aztec	3718.6	49,950	100,400	Barite	26.4	10.3						
Late breccia stage														
317-1156		Tewksbury	3287.7	50,747	100,205	Kaolinite				−115	9.0	−5.2/2.2	91.5/97.5	*100/200*
257-214		Annie	3586.3	51,886	99,703	Kaolinite				−93	14.4	0.1/7.1	69.5/76.5	*100/200*
332-257		Tewksbury	3592.3	50,819	100,145	Kaolinite					15.0	0.7/7.7		*100/200*
66-115		Annie	3616.5	51,881	99,705	Kaolinite				−89			65.5/72.5	*100/200*
Late alunite veins														
SUM-1-88a		Annie	3566.2	*52,100*	*99,700*	Alunite	24.5	13.4	8.6	−46		2.53	−37	*200/250*
328-108		Annie	3584.0	51,785	100,009	Alunite	13.4	9.9	7.6	−65		−0.97	−56	*200/250*

[a] Sample numbers in italics indicate outcrop or dump samples.
[b] Values in bold are direct determinations of δD from fluid-inclusion analysis.
[c] Temperatures in italics are assumed for fluid calculations; others are calculated from isotope data.
[d] 780 °C temperature.

References

Arribas Jr., A., 1995. Characteristics of high-sulfidation epithermal deposits, and their relation to magmatic fluid. In: Thompson, J.F.H. (Ed.), Magmas, Fluids, and Ore Deposits, Mineral. Assoc. Can. Short Course, vol. 23, pp. 419–454.

Arribas Jr., A., Cunningham, C.G., Rytuba, J.J., Rye, R.O., Kelly, W.C., Podwysocki, M.H., et al., 1995. Geology, geochronology, fluid inclusions and isotope geochemistry of the Rodalquilar Au-alunite deposit, Spain. Econ. Geol. 90, 795–822.

Ashley, R.P., 1974. Goldfield mining district. Rep. Nev. Bur. Mines Geol. 19, 49–66.

Ashley, R.P., 1982. Occurrence model for enargite–gold deposits. Open-File Rep. (U. S. Geol. Surv.) 82-0795, 144–147.

Barton Jr., P.B., Skinner, B.J., 1979. Sulfide mineral stabilities. In: Barnes, H.L. (Ed.), Geochemistry of Hydrothermal Ore Deposits, 2nd ed. Wiley, New York, NY, pp. 278–403.

Berger, B.R., 1986. Descriptive model of epithermal quartz–alunite Au. In: Cox, D.P., Singer, D.A. (Eds.), Mineral Deposit Models, U.S. Geol. Surv. Bull., vol. 1693, p. 158.

Berger, B.R., Henley, R.W., 1989. Advances in the understanding of epithermal gold–silver deposits, with special reference to the Western United States. Econ. Geol. Monogr. 6, 405–423.

Bethke, P.M., 1984. Controls on base- and precious-metal mineralization in deeper epithermal environments. Open-File Rep. (U. S. Geol. Surv.), 84–890.

Bodnar, R.J., 1993. Revised equation and table for determining the freezing point depression of H_2O–NaCl solutions. Geochim. Cosmochim. Acta 57, 683–684.

Bodnar, R.J., Burnham, C.W., Sterner, S.M., 1985. Synthetic fluid inclusions in natural quartz: III. Determination of phase equilibrium properties in the system H_2O–NaCl to 1000 °C and 1500 bars. Geochim. Cosmochim. Acta 49, 1861–1873.

Bottinga, Y., Javoy, M., 1973. Comments on oxygen isotope geothermometry. Earth Planet. Sci. Lett. 20, 251–265.

Bove, D.J., Rye, R.O., Hon, K., 1990. Evolution of the Red Mountain alunite deposit, Lake City, Colorado. Open-File Rep. (U. S. Geol. Surv.) 90-0235, 1–30.

Bruha, D.I., Noble, D.C., 1983. Hypogene quartz–alunite±pyrite alteration formed by moderately saline, ascendant hydrothermal solutions. Abstr. Programs-Geol. Soc. Am. 15 (5), 325.

Burnham, C.W., 1979. Magmas and hydrothermal fluids. In: Barnes, H.L. (Ed.), Geochemistry of Hydrothermal Ore Deposits, 2nd ed. Wiley, New York, pp. 263–277.

Criss, R.E., Gregory, R.T., Taylor Jr., H.P., 1987. Kinetic theory of oxygen isotopic exchange between minerals and water. Geochim. Cosmochim. Acta 51, 1099–1108.

Cunningham, C.G., 1985. Characteristics of boiling—water-table and carbon dioxide models for epithermal gold deposition. In: Tooker, E.W. (Ed.), Geologic Characteristics Of Sediment-And Volcanic-hosted Disseminated Gold Deposits—Search For An Occurrence Model., U.S. Geol. Surv. Bull., vol. 1646, pp. 43–46.

Deen, J.A., 1990. Hydrothermal ore deposition related to high-level igneous activity: a stable-isotope study of the Julcani mining district, Peru. PhD thesis, Univ. Colorado, Boulder, Colorado.

Deen, J.A., Rye, R.O., Munoz, J.L., Drexler, J.W., 1994. The magmatic hydrothermal system at Julcani, Peru: evidence from fluid inclusions and hydrogen and oxygen isotopes. Econ. Geol. 89, 1924–1938.

Deyell, C.L., Rye, R.O., Landis, G.P., Bissig, T., 2005. Alunite and the role of magmatic fluids in the Tambo high-sulfidation deposit, El Indio-Pascua belt, Chile. Chem. Geol. 215, 185–218 (this issue).

Dubé, B., Dunning, G., Lauzière, K., 1998. Geology of the Hope Brook mine, Newfoundland, Canada: a preserved late Proterozoic high-sulfidation epithermal gold deposit and its implications for exploration. Econ. Geol. 93, 405–436.

Ebert, S.W., Rye, R.O., 1997. Secondary precious metal enrichment by steam-heated fluids in the Crofoot-Lewis hot spring gold–silver deposit and relation to paleoclimate. Econ. Geol. 92, 578–600.

Enders, M.S., Coolbaugh, M.F., 1987. The Summitville gold mining district, San Juan Mountains, Colorado. Denver Region Exploration Geologists Society Fall Field Guidebook, pp. 28–36. 19–20, Sept.

Fifarek, R.H., Rye, R.O., 2005. Stable-isotope geochemistry of the Pierina high-sulfidation Au–Ag deposit, Peru: influence of hydrodynamics on lithological control of hydrodynamics on SO_4^{2-}–H_2S isotopic exchange in magmatic-steam and steam-heated environments. Chem. Geol. 215, 253–279 (this issue).

Foley, N.K., Bethke, P.M., Rye, R.O., 1990. A reinterpretation of the differences in hydrogen and isotopic composition of inclusion fluids in quartz and sphalerite from the Creede mining district, Colorado: a generic problem for shallow orebodies? Econ. Geol. 87, 1966–1977.

Fournier, R.O., 1987. Conceptual model of brine evolution. U. S. Geol. Surv. Prof. Pap. 1350 (2), 1487–1506.

Fournier, R.O., 1992. The influences of depth of burial and the brittle–plastic transition on the evolution of magmatic fluids. Rep., Geol. Surv. Jpn. 279, 57–59.

Fournier, R.O., 1999. Hydrothermal processes related to movement of fluid from plastic into brittle rock in the magmatic-hydrothermal environment. Econ. Geol. 94, 1193–1212.

Getahun, A., 1994. Fluid–rock reaction and mineralization in two high-level volcanic settings: Augustine fumaroles and the Summitville acid-sulfate copper–gold deposit. PhD thesis, University of Oregon, Eugene, Oregon.

Giggenbach, W.F., 1992. Magma degassing and mineral deposition in hydrothermal systems along convergent plate boundaries. Econ. Geol. 87, 1927–1944.

Giggenbach, W.F., 1997. The origin and evolution of fluids in magmatic-hydrothermal systems. In: Barnes, H.L. (Ed.), Geochemistry of Hydrothermal Ore Deposits, 3rd ed. Wiley, New York, pp. 737–796.

Gilg, H.A., Sheppard, S.M.F., 1996. Hydrogen isotopic fractionation between kaolinite and water revisited. Geochim. Cosmochim. Acta 60, 529–533.

Gray, J.E., Coolbaugh, M.F., 1994. Geology and geochemistry of Summitville, Colorado: an epithermal acid sulfate deposit in a volcanic dome. Econ. Geol. 89, 1906–1923.

Gray, J.E., Coolbaugh, M.F., Plumlee, G.S., Atkinson, W.W., 1994. Environmental geology of the Summitville mine, Colorado. Econ. Geol. 89, 2006–2014.

Gregory, R.T., Criss, R.E., 1986. Isotopic exchange in open and closed systems. In: Valley, J.W., Taylor Jr., H.P., O'Neil, J.R. (Eds.), Stable Isotopes in High Temperature Geological Processes, Rev. Mineral., vol. 16, pp. 91–127.

Haas Jr., J.L., 1976. Thermodynamic properties of the coexisting phases and thermochemical properties of the NaCl component in boiling NaCl solutions. U. S. Geol. Surv. Prof. Pap., 1-B71.

Hayba, D.O., Bethke, P.M., Heald, P., Foley, N.K., 1985. Geologic, mineralogic, and geochemical characteristics of volcanic-hosted epithermal precious-metal deposits. In: Berger, B.R., Bethke, P.M. (Eds.), Geology and Geochemistry of Epithermal Systems, Rev. Econ. Geol., vol. 2, pp. 129–167.

Heald-Wetlaufer, P., Foley, N.K., Hayba, D.O., 1987. Comparative anatomy of volcanic-hosted epithermal deposits. Acid-sulfate and adularia-sericite types. Econ. Geol. 82, 1–26.

Hedenquist, J.W., 1987. Mineralization associated with volcanic-related hydrothermal systems in the Circum-Pacific basin. In: Horn, M.K. (Ed.), Transactions of the Fourth Circum-Pacific Energy and Mineral Resources Conference. August 1986, Singapore, Am. Assoc. Petrol. Geol., Tulsa, Oklahoma, pp. 513–524.

Hedenquist, J.W., Lowenstern, J.B., 1994. The role of magmas in the formation of hydrothermal ore deposits. Nature 370, 519–527.

Hedenquist, J.W., Matsuhisa, Y., Izawa, E., White, N.C., Giggenbach, W.F., Aoki, M., 1994. Geology, geochemistry, and origin of high-sulfidation Cu–Au mineralization in the Nansatsu district, Japan. Econ. Geol. 89, 1–30.

Hedenquist, J.W., Arribas Jr., A., Reynolds, J.T., 1998. Evolution of an intrusion-centered hydrothermal system: Far Southeast-Lepanto porphyry and epithermal Cu–Au deposits, Philippines. Econ. Geol. 93, 373–404.

Henley, R.W., McNabb, A., 1978. Magmatic vapor plumes and ground-water interaction in porphyry copper emplacement. Econ. Geol. 73, 1–20.

Hills, R.C., 1885. Ore deposits of Summit District, Rio Grande County, Colorado. Colo. Sci. Soc. Proc. 1, 20–37.

Holland, H.D., Malinin, S.D., 1979. The solubility and occurrence of non-ore minerals. In: Barnes, H.L. (Ed.), Geochemistry of Hydrothermal Ore Deposits, 2nd ed. Wiley, New York, pp. 461–508.

Huang, C.K., 1955. Gold copper deposits of the Chinkuashih mine, Taiwan, with special reference to the mineralogy. Acta Geol. Taiwanica 7, 1–20.

Juliani, C., Rye, R.O., Nunes, C.M.D., Snee, L.W., Correa Silva, R.H., Monteiro, L.V.S., 2005. Paleoproterozoic high-sulfidation mineralization in the Tapajós gold province, Amazonian craton, Brazil: geology, mineralogy, alunite argon age, and stable-isotope constraints. Chem. Geol. 215, 95–125 (this issue).

Kharaka, Y.K., O'Neil, J.R., 1976. Hydrogen isotope exchange between clay minerals and water. Geochim. Cosmochim. Acta 40, 241–246.

Larson, P.T., Taylor, H.P., 1987. Solfataric alteration in the San Juan Mountains, Colorado: oxygen isotope variations in a boiling hydrothermal environment. Econ. Geol. 82, 1019–1036.

Mehnert, H.H., Lipman, P.W., Steven, T.A., 1973. Age of mineralization at Summitville, Colorado as indicated by K–Ar dating of alunite. Econ. Geol. 67, 214–230.

Muntean, J.L., Einaudi, M.T., 2001. Porphyry–epithermal transition: Maricunga Belt, Northern Chile. Econ. Geol. 96, 743–772.

Ohmoto, H., Lasaga, A., 1982. Kinetics of reactions between aqueous sulfates and sulfides in hydrothermal systems. Geochim. Cosmochim. Acta 46, 1727–1745.

Ohmoto, H., Rye, R.O., 1974. Hydrogen and oxygen isotopic compositions of fluid inclusions in the Kuroko deposits, Japan. Econ. Geol. 69, 947–953.

Ohmoto, H., Rye, R.O., 1979. Isotopes of sulfur and carbon. In: Barnes, H.L. (Ed.), Geochemistry of Hydrothermal Ore Deposits, 2nd ed. Wiley, New York, pp. 509–567.

O'Neil, J.R., Chappell, B.W., 1977. Oxygen and hydrogen isotope relations in the Berridale Batholith. J. Geol. Soc. (Lond.) 133, 559–571.

Patton, H.B., 1917. Geology and ore deposits of the Platoro–Summitville mining district, Colorado. Colorado Geol. Surv. Bull. 13, 1–132.

Reed, M., Spycher, N., 1986. Calculation of pH and mineral equilibria in hydrothermal waters and application to geothermometry and studies of boiling and dilution. Geochim. Cosmochim. Acta 48, 1479–1492.

Rye, R.O., 1993. The evolution of magmatic fluids in the epithermal environment: the stable isotope perspective: SEG distinguished lecture. Econ. Geol. 88, 733–753.

Rye, R.O., 2005. A review of the stable-isotope geochemistry of sulfate minerals in selected igneous environments and related hydrothermal systems. Chem. Geol. 215, 5–36 (this issue).

Rye, R.O., Bethke, P.M., Wasserman, M.D., 1989. Diverse origins of alunite and acid-sulfate alteration: stable isotope systematics. Open-File Rep. (U. S. Geol. Surv.), 89–95.

Rye, R.O., Stoffregen, R.E., Bethke, P.M., 1990. Stable isotope systematics and magmatic and hydrothermal processes in the Summitville, CO, gold deposit. Open-File Rep. (U. S. Geol. Surv.), 90–626.

Rye, R.O., Bethke, P.M., Wasserman, M.D., 1992. The stable isotope geochemistry of alunite. Econ. Geol. 87, 225–262.

Scott, K.M., 1990. Origin of alunite- and jarosite-group minerals in the Mt. Leyshon epithermal gold deposit, Northeast Queensland, Australia. Am. Mineral. 75, 1176–1181.

Sheppard, S.M.F., Gilg, H.A., 1996. Stable isotope geochemistry of clay minerals. Clay Miner. 31, 1–24.

Sillitoe, R.H., 1973. The tops and bottoms of porphyry copper deposits. Econ. Geol. 68, 799–815.

Sillitoe, R.H., 1983. Enargite-bearing massive sulfide deposits high in porphyry copper systems. Econ. Geol. 78, 348–352.

Sillitoe, R.H., 1989. Gold deposits in western Pacific island arcs; the magmatic connection. In: Keays, R.R., Ramsay, W.R.H., Groves, D.I. (Eds.), The Geology of Gold Deposits; the Perspective in 1988, Econ. Geol. Monogr., vol. 6, pp. 274–291.

Sillitoe, 1995. The influence of magmatic-hydrothermal models on exploration strategies for volcano–plutonic arcs. In: Thompson, J.F.H. (Ed.), Magmas, Fluids, and Ore Deposits, Mineral. Assoc. Can. Short Course, vol. 23, pp. 511–525.

Sourirajan, S., Kennedy, G.C., 1962. The system H_2O–NaCl at elevated temperatures and pressures. Am. J. Sci. 260, 115–141.

Steven, T.A., Ratté, J.C., 1960. Geology and ore deposits of the Summitville district, San Juan Mountains, Colorado. U. S. Geol. Surv. Prof. Pap. 487, 1–9.

Steven, T.A., Lipman, P.W., 1976. Calderas of the San Juan volcanic field, Southwestern Colorado. U. S. Geol. Surv. Prof. Pap. 958, 1–35.

Stoffregen, R.E., 1985. Genesis of acid-sulfate alteration and Cu–Au–Ag mineralization at Summitville, Colorado (including sections on supergene alteration and clay mineralogy of the deposit). PhD thesis, Univ. California, Berkeley, California.

Stoffregen, R.E., 1986. Observations on the behavior of gold during supergene oxidation at Summitville, Colorado, and implications for electrum stability in the weathering environment. Appl. Geochem. 1, 549–558.

Stoffregen, R.E., 1987. Genesis of acid-sulfate alteration and Cu–Au–Ag mineralization at Summitville, Colorado. Econ. Geol. 82, 1575–1591.

Stoffregen, R.E., Rye, R.O., Wasserman, M.D., 1994. Experimental studies of alunite: II. ^{18}O–^{16}O and D–H fractionation factors between alunite and water at 250–450 °C. Geochim. Cosmochim. Acta 58, 903–916.

Stoffregen, R.E., Vikre, R.E., Bethke, P.G., 2004. Homogenization temperature and salinity data for fluid inclusions from the Summitville, Colorado Cu–Au–Ag deposit. Open-File Rep. (U. S. Geol. Surv.) 2004-1066, 1–14.

Taylor, Jr., H.P., 1974. Oxygen and hydrogen isotope evidence for large-scale circulation and interaction between ground waters and igneous intrusions with particular reference to the San Juan volcanic field, Colorado. In: Hofmann, A.W., Giletti, B.J., Yoder, H.S. Jr., Yund, R.A. (Eds.), Geochemical Transport and Kinetics. Carnegie Inst. Wash. Pub. 634, 299–334.

Taylor Jr., H.P., 1979. Oxygen and hydrogen isotope relationships in hydrothermal mineral deposits. In: Barnes, H.L. (Ed.), Geochemistry of Hydrothermal Ore Deposits, 2nd ed. Wiley, New York, pp. 236–277.

Taylor, B.E., 1992. Degassing of H_2O from rhyolitic magma during eruption and shallow intrusion, and isotopic composition of magmatic water in hydrothermal systems. Rep., Geol. Surv. Jpn. 279, 190–194.

Tuttle, M.L., Goldhaber, M.B., Williamson, D.L., 1986. An analytical scheme for determining forms of sulfur in oil shales and associated rocks. Talanta 33, 953–961.

Ueda, A., Sakai, H., 1984. Sulfur isotope study of Quaternary volcanic rocks from the Japanese Islands Arc. Geochim. Cosmochim. Acta 48, 1837–1848.

Vikre, P.G., 1990. Ledge formation at the Sandstorm and Kendall gold mines, Goldfield, Nevada. Econ. Geol. 84, 2115–2138.

Wasserman, M.D., Rye, R.O., Bethke, P.M., Arribas Jr., A., 1992. Methods for separation and total stable isotope analysis of alunite. Open-File Rep. (U. S. Geol. Surv.), 92–99.

Watanabe, Y., Hedenquist, J.W., 2001. Mineralogic and stable isotope zonation at the surface over the El Salvador porphyry copper deposit, Chile. Econ. Geol. 96, 1775–1797.

White, N.C., 1991. High sulfidation epithermal gold deposits: characteristics, and a model for their origin. Rep., Geol. Surv. Jpn. 227, 9–20.

White, N.C., Hedenquist, J.W., 1995. Epithermal gold deposits: styles, characteristics and exploration. Soc. Econ. Geol. Newsl. 21 (1), 9–13.